Journal of Sound and Vibration 403 (2017) 190–213

Contents lists available at ScienceDirect

Journal of Sound and Vibration

journal homepage: www.elsevier.com/locate/jsvi

On a two-dimensional mode-matching technique for sound generation and transmission in axial-flow outlet guide vanes

Simon Bouley [a], Benjamin François [a], Michel Roger [a,*], Hélène Posson [b], Stéphane Moreau [c]

[a] École Centrale de Lyon, Laboratoire de Mécanique des Fluides et Acoustique, UMR CNRS 5509, 36, avenue Guy de Collongue, Écully 69143, France
[b] Airbus Operations S.A.S., 316, Route de Bayonne, Toulouse Cedex 09, 31060, France
[c] Département de Génie Mécanique, Université de Sherbrooke, Sherbrooke, QC, Canada J1K2R1

A R T I C L E I N F O

Article history:
Received 14 December 2016
Received in revised form
23 March 2017
Accepted 24 April 2017
Handling Editor: P. Joseph

Keywords:
Axial-flow fan stage
Rotor-stator wake-interaction noise
Sound generation
Sound transmission
Mode-matching technique
Cascade effect

A B S T R A C T

The present work deals with the analytical modeling of two aspects of outlet guide vane aeroacoustics in axial-flow fan and compressor rotor-stator stages. The first addressed mechanism is the downstream transmission of rotor noise through the outlet guide vanes, the second one is the sound generation by the impingement of the rotor wakes on the vanes. The elementary prescribed excitation of the stator is an acoustic wave in the first case and a hydrodynamic gust in the second case. The solution for the response of the stator is derived using the same unified approach in both cases, within the scope of a linearized and compressible inviscid theory. It is provided by a mode-matching technique: modal expressions are written in the various sub-domains upstream and downstream of the stator as well as inside the inter-vane channels, and matched according to the conservation laws of fluid dynamics. This quite simple approach is uniformly valid in the whole range of subsonic Mach numbers and frequencies. It is presented for a two-dimensional rectilinear-cascade of zero-staggered flat-plate vanes and completed by the implementation of a Kutta condition. It is then validated in sound generation and transmission test cases by comparing with a previously reported model based on the Wiener-Hopf technique and with reference numerical simulations. Finally it is used to analyze the tonal rotor-stator interaction noise in a typical low-speed fan architecture. The interest of the mode-matching technique is that it could be easily transposed to a three-dimensional annular cascade in cylindrical coordinates in a future work. This makes it an attractive alternative to the classical strip-theory approach.

1. Introduction

Axial-flow turbomachines are known as key contributors to the aerodynamic noise of modern aircrafts, from the standpoint of the propulsive systems causing environmental issues as well as from the standpoint of air-conditioning units involved in cabin comfort. Dealing with external noise, the evolution of modern turbofan engines toward larger bypass ratios in the past decades has led to a continuous jet-noise reduction, making rotating-blade noise the dominant

* Corresponding author.
E-mail addresses: michel.roger@ec-lyon.fr (M. Roger), stephane.moreau@usherbrooke.ca (S. Moreau).

http://dx.doi.org/10.1016/j.jsv.2017.04.031

Nomenclature

Latin characters

a	Inter-vane channel width
A_j	Vortical inter-vane channel coefficient
B	Rotor blade number
B_n	Vortical transmission coefficient
C	Vane chord
c_o	Sound speed
D_q	Acoustic downstream channel coefficient
k	Acoustic wavenumber
$k^{\pm}$	Generic axial acoustic wavenumber
k_n	Acoustic wave number at the n-th BPF order
M	Axial Mach number
M_t	Tangential Mach number
(r, θ, x)	Cylindrical duct coordinates
R_0	Radius of a cylindrical cut
R_s	Acoustic reflection coefficient
T_s	Acoustic transmission coefficient
u	Inter-vane phase angle
U_q	Acoustic upstream channel coefficient
V	Stator vane number
V_j	Vortical coefficient induced by the Kutta condition
(x, y, z)	Cartesian coordinates
w	Generic wake velocity-deficit notation
W_x	Axial mean-flow velocity

Greek characters

α	Generic azimuthal wave number
β	Compressibility factor
β_r	Rotor exit-flow angle
$\mathbf{\Gamma}$	Pressure-axial velocity vector
Θ	Angle of propagation of the incident acoustic wave
$\underline{\boldsymbol{\varphi}}$, $\underline{\mathbf{\Psi}}$	Modal projection constants
ρ_0	Mean fluid density
σ	Solidity
ϕ	Acoustic potential
ω	Angular frequency
Ω	Rotor rotational speed
Ω_0	Strength of the vortical Dirac delta function

Subscripts and superscripts

n	Blade-Passing Frequency (BPF) order index
m	Inter-vane channel index
i, r, d, u, t	Incident, reflected, downstream channel, upstream channel, transmitted components
μ, s, q, j, n_i	Modal orders
$+, -$	Superscripts for downstream/upstream propagating waves
$\mathbf{x}$	Vector
$\underline{\mathbf{x}}$	Matrix

contribution, especially during approach and landing operation. More precisely the fan and its outlet guide vanes (OGV) in the annular duct are recognized as the main sources of noise. Dealing with internal noise, the contribution of the small-size ducted fans used in on-board air-conditioning circuits tends to grow in terms of relative levels, especially as a lower propulsion noise is transmitted inside the cabin. Facing this new context and the more and more stringent requirements in terms of noise reduction, the understanding and the modeling of the noise-generating mechanisms are crucial needs for aircraft manufacturers and equipment suppliers.

The common features of the turbofan and air-conditioning fan can be reduced to a single sound-producing rotor-stator stage, with ideally an axial mean flow upstream of the rotor and downstream of the OGV (see Fig. 1). Elucidating the role of the OGV in the aeroacoustic behavior of the stage is the main motivation of the present work. As long as the rotor-stator distance is large enough to avoid the strong coupling that takes place when the leading edges of the stator vanes enter the near-wake region of the rotor blades, this role is twofold and can be analyzed as follows. Firstly the wakes issuing from the rotor impinge on the vanes, inducing unsteady loads that are responsible for what is referred to as wake-interaction noise.

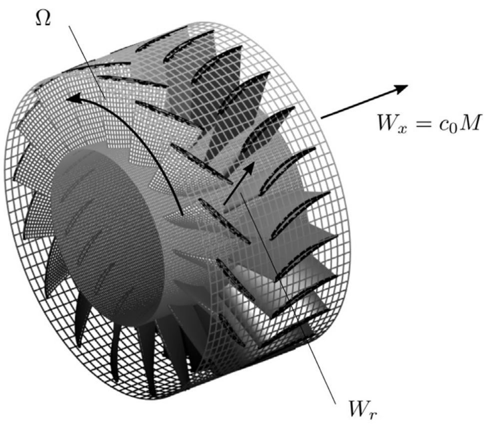

Fig. 1. Typical axial-flow fan stage used in air-conditioning systems for aircraft, featuring the rotor rotating in the counter-clockwise direction and the stator (outlet guide vanes).

Secondly the acoustic waves generated by the rotor blades are restructured by their transmission through the stator before propagating in the exhaust duct. Both mechanisms hold for the tonal noise associated with the periodic aerodynamic phenomena and for the broadband noise associated with the turbulent part of the flow.

For a preliminary acoustic design of the stage, resorting to a fully numerical simulation of the flow is not appropriate because details of the blade and vane cross-sections can still be unknown, on the one hand, and because many configurations can need to be tested for the sake of optimization, on the other hand. Fast-running analytical tools with a reasonable accuracy are better suited. Furthermore they make the physical understanding easier, which is very attractive for the definition of low-noise design rules. This is why the analytical approach is chosen here.

As a price to pay for the simplicity, analytical modeling requires drastic approximations on the blade/vane geometry and on the flow features in order that the solving of the mathematical problem remains tractable and produces closed-form solutions. Decisive choices have to be accepted, even if the blades/vanes are simplified as rigid flat plates of zero thickness embedded in a uniform mean flow. It is assumed here that the cascade effect of a blade or vane row is the dominant feature, more crucial than the precise geometry of the blades/vanes. The cascade effect is defined as the effect of adjacent blades/vanes on the response of a reference blade/vane to either aerodynamic or acoustic excitation. It is a matter of number of blades/vanes, stagger angle and solidity and has already been recognized by many authors, amongst others Goldstein [1], Atassi and Hamad [2], Hall and Silkowski [3] and Peake and Parry [4] for instance. The question is considered only for the stator, firstly for simplicity in order to demonstrate the effectiveness of the proposed methodology, and secondly because the cascade effect is more pronounced than for a rotor. Because the exit flow from the outlet guide vanes must be axial, the aft part of the vanes is nearly aligned with the axis. The vanes are also inclined at the leading edge and moderately cambered in such a way that they have a large overlap. In the present two-dimensional approach, the stator is therefore unwrapped and represented by an infinite rectilinear cascade of parallel and axially aligned flat plates of zero-thickness. This simplification is similar to the classical assumption made in the linearized unsteady aerodynamic theory for thin airfoils [5]. As a consequence the inter-vane channels can be equivalently considered as a periodic array of bifurcated waveguides with rigid walls.

In the 1970s, the growing development of turbomachinery in aeronautic engineering led to a great deal of effort to understand and model the sound production in rotating and stationary blade/vane rows. Numerical and analytical studies were carried out to model two-dimensional rectilinear cascades of flat plates. Kaji and Okazaki [6] considered the sound transmission through a blade row, by considering each blade as an unsteady distribution of dipole sources and using a singularity method based on the acceleration potential. The same method was used to model the generation of rotor-stator interaction noise in a following paper [7]. A similar technique was used by Carta [8] who only considered the acoustic resonance or cut-off in the cascade of vanes. Whitehead [9], then Smith [10], developed a model based on a lifting-surface method which gives the unsteady loading, the vortical field and the acoustic field upstream and downstream of a two-dimensional blade row for any type of incident acoustic wave or vortical gust or bending or torsional vibration. Then Whitehead [11] implemented this formulation in the code LINSUB. The first model of a three-dimensional rectilinear cascade with duct walls was attempted by Goldstein [1] and readdressed by Atassi and Hamad [2] to formulate the impingement of wakes on a blade row. Most of these solutions require to solve an integral equation with a collocation technique, then they resort to a numerical implementation.

Alternatively, the Wiener-Hopf technique has been extensively applied to provide explicit solutions in the two-dimensional rectilinear cascade configuration. Mani and Horvay [12] considered the sound transmission through an infinite array of semi-infinite flat plates, neglecting the back-scattering by the trailing edges, and used an approximate solution based on the Wiener-Hopf technique. Koch [13] extended this analysis to blades of finite chord and gave expressions for the transmission and reflection factors for both upstream and downstream propagating acoustic waves. This full formulation is accurate but remains computationally time-consuming. In this context, Peake [14] extended Koch's formulation to the impingement of a two-dimensional vortical gust and determined the unsteady loading on the blades. He also developed a high-frequency approximation that enables a quick evaluation of the functions needed in the Wiener-Hopf technique [15]. Glegg [16] used the Wiener-Hopf technique to derive the exact solution for the acoustic field radiated from a three-dimensional rectilinear cascade, excited by a three-dimensional acoustic wave or a vortical gust. The calculation did not require the determination of the field inside the cascade. More recently, Posson et al. [17] completed this approach to provide exact expressions for the acoustic field inside the inter-blade channels and for the pressure jump over the blades, in a subsonic mean flow. When applied to thin annular unwrapped cuts of a true stator within the scope of a strip-theory approach, this technique is able to take into account three-dimensional blade/vane design parameters such as twist, lean and sweep. However the results it produces can deviate substantially from those of three-dimensional approaches such as the lifting surface theory, for instance, as pointed out by Namba [18]. Elhadidi and Atassi [19] and Posson et al. [20] also stressed that resorting to a strip-theory approach with Glegg's solution to model a three-dimensional annular cascade introduces non physical artifacts. Firstly, the unwrapped configuration implies an abusive parallelism between adjacent vanes, which tends to emphasize resonance effects. Such a deficiency has been improved by introducing a correction on the unsteady blade loading to account for the dispersion relationship of annular duct modes in the rectilinear-cascade model [21]. Secondly, the strip-theory approach does not account for the modal scattering into radial orders. This means that the cascade effect at a given radius is calculated ignoring multiple reflections at other radii. Finally artificial jumps of phase and amplitude between adjacent strips are generated, modifying the cut-off properties from one strip to another.

Mathematically equivalent, the mode-matching technique has been widely used to formulate boundary-value problems in the theory of electromagnetic waves. It is well suited to describe discontinuities or bifurcations in waveguide systems of various geometries since it consists in matching modal expansions of the fields in the different sub-domains bounded by the vanes, provided that explicit expressions are known for the modes. It is described in details in the reference handbook by Mittra and Lee [22]. A key application with a staggered array of semi-infinite plates has been proposed by Whitehead [23] for electromagnetic wave scattering. Linton and Evans [24] appear to be the first who applied the mathematical formalism developed by Mittra and Lee to the acoustic scattering by a two-dimensional array of zero-stagger parallel plates in a medium at rest. Assuming a high solidity and using the residue theorem, they presented expressions for the reflection and transmission modal amplitudes. This work led to the study of trapped modes and acoustic resonances in a two-dimensional waveguide (Evans [25]), in an array of finite thin plates with a mean flow (Duan [26]) and in cylindrical waveguides (Duan et al. [27]). Nayfeh and Huddleston [28] investigated the particular configuration of the trapped modes (or Parker's modes [29]) around a finite thin plate in a two-dimensional duct in absence of flow. Duan [26] solved the same problem adding a uniform subsonic flow, again using the same mode-matching technique and the residue calculus theory. The numerical results were found in an excellent agreement with Koch's results [30] obtained with the Wiener-Hopf technique. Roger [31] and later Roger et al. [32] applied the mode-matching technique to a simplified two-dimensional configuration of centrifugal compressor in polar coordinates, assimilating the vanes of a radial diffuser to radial rigid plates. For this, spiral acoustic modes in a spiral base-flow were introduced. Ingenito and Roger [33] also addressed the problem of sound transmission at the interface between an annular array of semi-infinite channels and an annular duct in a uniform axial flow.

The mode-matching technique, considered in the present work, is thus conceptually different. The main advantage is that it can be transposed directly in various coordinate systems, as long as the Helmholtz equation remains separable in each sub-domain. In particular it can be applied in cylindrical coordinates to address the configuration of an annular cascade, by introducing the Bessel functions as radial shape functions for the elementary waves. This avoids the artificial splitting into radial strips. The counterpart is that the formalism *a priori* holds only for straight, zero-stagger radial vanes. The two-dimensional extension of the mode matching to staggered vanes is possible following the similar case of the scattering of electromagnetic waves by optical gratings [23], as long as adjacent vanes have a non-zero overlap, which just makes it an alternative to the aforementioned Wiener-Hopf technique. Up to that point both techniques can be used in a strip-theory approach and both will remain attractive till some more general statement is available. Their equivalence is used to validate the implementation of the mode-matching technique in the present study which must be considered as a needed preliminary step for further extensions. It must be noted that actual blade design parameters have been recognized as important for the prediction of cascade tonal noise whereas they are not essential for the prediction of the broadband noise [34]. This suggests that the present study based on the assumption of flat-plate vanes, as well as other similar statements, is more relevant for the latter than for the former. Yet it remains an alternative when the design parameters are not known.

The present work extends the use of the mode-matching technique in a unified approach to address sound-generating and sound-transmission phenomena in a two-dimensional cascade of zero-stagger vanes. This includes the presence of flow and the implementation of a Kutta condition. The two-dimensional declination must be understood as a preliminary step aimed at assessing the robustness of the implementation. The extensions to three-dimensional configurations are the matter for a future work. The first attempts were described in a previous paper by Bouley et al. [35]. A two-dimensional model of cascade trailing-edge noise partly based on the same mode-matching strategy has also been described recently by Roger et al. [36].

The present study aims at modeling analytically the sound generation and transmission in a two-dimensional row of overlapping vanes in the frequency domain, by means of the mode-matching technique. The underlying principles of the mode-matching technique are detailed in Section 2. The technique is first applied to the diffraction of an incident acoustic wave by a cascade of vanes in Section 3. The solving procedure is detailed and the mechanisms of wave scattering by the two interfaces are highlighted. The implementation of a Kutta condition at the trailing edges of the vanes is also described. Sample results and a comparison with the Wiener-Hopf technique are provided. The impingement of a vortical gust on the cascade is studied in Section 4 as a background for the formulation of rotor-stator wake-impingement noise. The wake modeling and the matching equations are presented. A test case extracted from the NASA Second computational aeroacoustic workshop Category 3 on benchmark problems is used to validate the present formulation. Finally the model is applied to understand some features of the rotor-stator interaction noise in a realistic low-speed fan, in view of the compared blade and vane counts.

2. Mode-matching technique, basic principles

2.1. Basic assumptions

The fluid is assumed inviscid and not heat-conducting, with uniform and constant entropy. The fluctuations of velocity, pressure and density are solutions of the linearized Euler equations. The mean-flow velocity is axial, uniform and subsonic of Mach number M. A typical axial-flow fan stage as depicted in Fig. 1 is reduced to some cylindrical cut of radius R_0 (Fig. 2-a) in which the vanes are assimilated to rigid flat plates of zero thickness and stagger. This cut is unwrapped to be described as a two-dimensional infinite rectilinear cascades in Cartesian coordinates (Fig. 2-b). Equivalently, the cascade is considered as a periodic array of bifurcated waveguides of length c and width $a = 2\pi R_0/V$, where V is the number of vanes. This defines

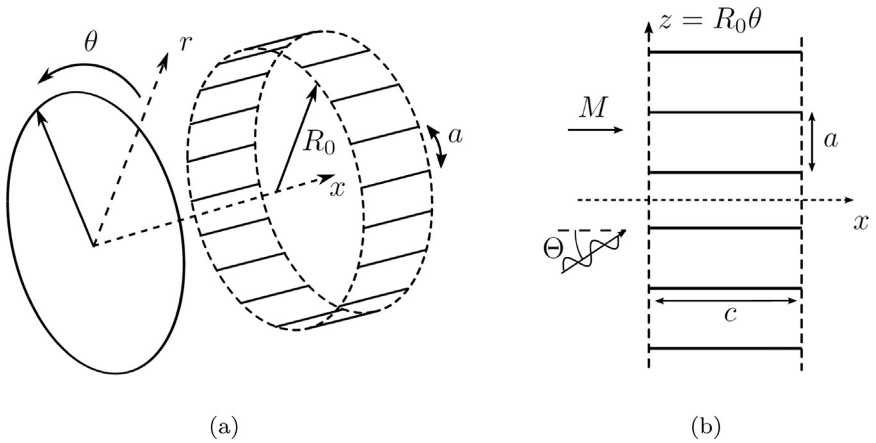

Fig. 2. (a): Geometrical reduction: cylindrical cut of radius R_0. (b): 2D unwrapped representation of the stator.

various sub-domains, namely the upstream and downstream open spaces in the regions $x < 0$ and $x > c$, respectively, and the series of inter-vane channels.

The application of the present two-dimensional model to real systems can be justified as follows. In two dimensions, a cascade impinged by incident waves produces oblique scattered waves, the angles of which are defined by the phase shifts between adjacent vanes (or blades). The re-emission angles combine with the orientation of the vanes. Because the secondary sources equivalent to the scattering are dipoles normal to the vane surfaces, they have a natural individual directivity, radiating at maximum level in quite a wide range of angles around their axis and having extinction in the plane normal to the axis. As long as a forced emission angle remains away from the angle of the extinction plane, an error on the stagger angle is acceptable. In other words the incident and scattered waves must not have directions of propagation that are close to the direction of the vanes. The angle of interest here corresponds to what would be the angle of helicity in an annular duct, corresponding to the azimuthal index of the modes. In the annular duct another angle can be defined in a meridian plane for some modes, related to the radial modal structure; this typically corresponds to reflections between the inner and outer walls. In order for the two-dimensional model to be representative of a real configuration, one of two situations must be encountered. The first one is when the annulus is very thin in terms of acoustic wavelengths, with a large hub-to-tip ratio, in which case the field tends to be homogeneous in the radial direction. This was demonstrated for instance in the case of propagation by Posson et al. with the Wiener-Hopf method [37]. The second one is when the annular propagation only takes place in a limited portion of the duct close to the outer wall. This so-called acoustic skin effect can be related to Chapman's caustic-radius theory and is encountered for high azimuthal modal orders in practice [38]. Finally it should also be stressed that assuming zero stagger is equivalent to neglect the swirl and its effects on upstream propagation, such as the shift in cut-off frequencies as noted by Cooper and Peake [39].

2.2. Jump conditions at an interface

In the mode-matching technique, the leading-edge and trailing-edge cross-sections of the stator are considered as interfaces at which physical quantities are matched to satisfy the basic conservation laws of fluid dynamics. The same principle holds in the original cylindrical coordinates (Fig. 2-a), as long as all points of a vane edge are approximately contained in the same cross-section, or in a Cartesian unwrapped representation of the vanes for a cut at radius $r = R_0$ (Fig. 2-b). The conservation laws correspond to jump conditions expressed on the mass-flow rate and either on the rothalpy (in a moving reference frame attached to a rotating blade) or on the total or stagnation enthalpy (for a stationary vane row) [32]. Here the conservation of the mass-flow rate leads to:

$$\left[\rho \mathbf{W}_1^2\right] \cdot \mathbf{n} = 0 \tag{1}$$

where the square brackets stand for the difference of a quantity between the sides 2 and 1 of the considered interface, the normal vector $\mathbf{n}$ pointing from side 1 to side 2. $(\rho, \mathbf{W})$ are the density and the absolute fluid-velocity fields in the stator reference frame. Viscosity and heat conduction are neglected. Therefore, the conservation of the stagnation enthalpy yields:

$$\left[H + \frac{\| \mathbf{W} \|^2}{2}\right]_1^2 = 0 \tag{2}$$

where $\|\bullet\|$ is the Euclidean norm of the vector. Writing the enthalpy H as a function of the temperature T and invoking the isentropic perfect-gas equations first leads to:

$$H = C_p T \quad \text{and} \quad T = T_0 + \frac{p}{\rho_0 C_p}$$

where C_p is the constant-pressure thermal capacity of the gas. The index zero refers to the steady-state variables and $(p, \rho, \mathbf{v})$ stand for the fluctuating pressure, density and velocity. After linearization Eq. (1) leads to the condition:

$$\left[Mp + \rho_0 c_0 \, \mathbf{v} \cdot \mathbf{e}_x\right]_1^2 = 0 \tag{3}$$

in which $M = W_x/c_0$ is the axial Mach number, c_0 is the speed of sound and $\mathbf{v} \cdot \mathbf{e}_x$ the disturbance velocity in the x (axial) direction. Eq. (2) leads to the second condition

$$\left[(1 - M^2) \, \mathbf{v} \cdot \mathbf{e}_x\right]_1^2 = 0 \tag{4}$$

In the present framework all mean-flow variables are assumed constant and equal on both sides of the interface, so that Eqs. (3) and (4) obviously reduce to the continuity of fluctuating pressure and axial velocity:

$$[p]_1^2 = 0, \quad \text{and} \quad [\mathbf{v} \cdot \mathbf{e}_x]_1^2 = 0. \tag{5}$$

These are classical conditions for the transmission of acoustic waves in axial bifurcated waveguides. But because the linearized equations of gas dynamics for a homogeneous base flow coincide with the convected wave equation they also hold when formulating the acoustic response of an interface to impinging vortical and pressure-free disturbances; this will be addressed in Section 4.

2.3. *Trace-velocity matching principle*

When formulating the mode-matching technique at an interface, modal expansions of the fluctuating pressure and axial velocity on both sides of the interface are required. All scattered waves must have a tangential/azimuthal phase speed along the interface that fits with the phase speed of the prescribed incident oblique wave. This is known as the trace-velocity matching principle, also involved in the generic problem of plane-wave transmission at the interface between two homogeneous fluids of different properties [40, 41].

Let the oblique two-dimensional incident wave be specified with the phase $e^{-i(\omega t - k_x x - k_z z)}$, where k_x and k_z are the axial and tangential wavenumbers, respectively. The 2π-periodicity on the variable $\theta = z/R_0$ implies that $2\pi R_0 = n\lambda_z$ or $k_z R_0 = n$ where $\lambda_z = 2\pi/k_z$ is the tangential wavelength and $|n|$, an integer, is the number of lobes. Because the angle of the plane wave can only take discrete values the wave is said a mode of the upstream region and n is said the mode order. The reflected waves of the form $e^{-i(\omega t - k_x^* x - k_z^* z)}$ must satisfy the same condition: $k_z^* R_0 = n^*$. The continuity of the tangential phase speed imposes that the phase shifts between two points in the z direction are the same for all waves. For the incident and reflected waves, they are given by $e^{i(2\pi n)/V}$ and $e^{i(2\pi n^*)/V}$, respectively, so that $n^* = n + sV$, $[n, s] \in \mathbb{Z}$. The same condition applies to the transmitted channel wave for which the phase-shift between adjacent channels must be equal to $e^{i(2\pi n)/V}$.

3. Diffraction of an acoustic wave by a cascade of vanes

The response of an unwrapped cascade of OGV, understood as a periodic array of bifurcated waveguides, to acoustic excitation *a priori* depends on dimensionless parameters (see Fig. 3). These are the acoustic wavelength to chord-length ratio λ/c, the acoustic-wavelength to inter-vane distance ratio λ/a and the solidity c/a. Typically if $\lambda/c \gg 1$ and $\lambda/a \gg 1$, the inter-vane channels are acoustically compact. In this case the incident wave is almost totally transmitted with a very weak reflection. If $\lambda/a > 2$, only the axial plane wave can propagate inside a channel. For other arbitrary values of the parameters multiple scattering between both interfaces leads to more or less complicated wave patterns. The present formulation holds for any configuration. It is based on general expressions of the acoustic potential fields in the individual regions (upstream, inter-vane channels, downstream) in terms of their respective modes.

3.1. *Definition of the acoustic potentials*

All acoustic potentials are noted $\phi(x, z)e^{-i\omega t}$ where ϕ has to satisfy the convected Helmholtz equation for a uniform axial flow of Mach number M:

$$\frac{\partial^2 \phi}{\partial z^2} + (1 - M^2)\frac{\partial^2 \phi}{\partial x^2} + 2ikM\frac{\partial \phi}{\partial x} + k^2\phi = 0, \tag{6}$$

introducing the acoustic wavenumber $k = \omega/c_0$. The acoustic pressure and velocity are related to the potential by the equations

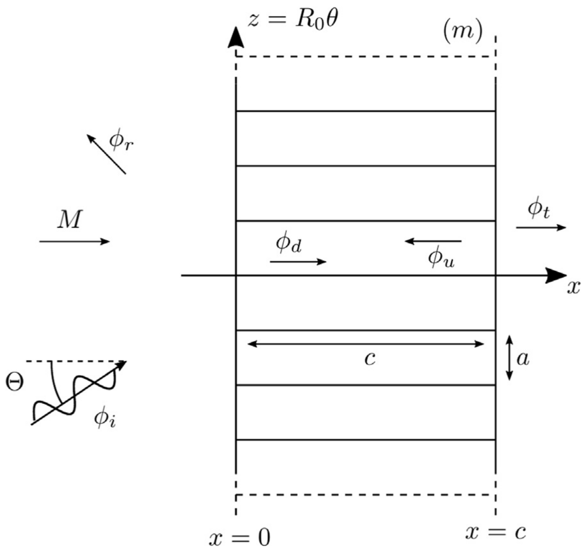

Fig. 3. Acoustic transmission through the OGV. Incident and scattered wave notations. 2D unwrapped representation.

$$p^{ac} = -\rho_0(-\mathrm{i}\omega\phi + \mathbf{W}\cdot\nabla\phi), \quad \mathbf{v}^{ac} = \nabla\phi\ ,$$

where $\mathbf{W} = W_x\mathbf{e}_x = Mc_0\mathbf{e}_x$ is the mean-flow velocity vector. The first application considered in the present work is the impingement of an oblique acoustic plane wave (or mode) of potential:

$$\phi_i = \mathrm{e}^{\mathrm{i}\alpha_i z}\mathrm{e}^{\mathrm{i}k_i^+ x}, \quad x \le 0 \tag{7}$$

with

$$\alpha_i = \frac{k\sin\Theta}{1 + M\cos\Theta}, \quad k_i^+ = \frac{-Mk + \overline{k_i}}{\beta^2}, \quad \overline{k_i} = \sqrt{k^2 - \beta^2\alpha_i^2}, \quad \beta = \sqrt{1 - M^2}.$$

Here $\overline{k_i}$ denotes the propagating part of the axial wavenumber and Θ is the angle of the incident mode with respect to the x-axis (see Fig. 3). The mode is assumed cut-on, which means that $\overline{k_i}$ is real. The 2π-periodicity imposes that $n = \alpha_i R_0 \in \mathbb{Z}$. Thus, more generally, the angle of propagation of a cut-on mode reads:

$$\Theta^{\pm} = \arccos\left(\frac{-\eta^2\,M \pm \sqrt{1 - \beta^2\eta^2}}{1 + \eta^2\,M^2}\right), \quad \text{with} \quad \eta = \frac{n}{kR_0}. \tag{8}$$

The $\pm$ symbol denotes the either upstream (-) or downstream $(+)$ propagation. Four acoustic fields are produced by the diffraction: the reflected and transmitted fields in the unbounded domains upstream and downstream of the cascade, denoted by their potentials ϕ_r and ϕ_t, and those in the inter-vane channels denoted by ϕ_u and ϕ_d with regard to their upstream and downstream propagation directions, respectively (Fig. 3). The reflected (ϕ_r) and the transmitted (ϕ_t) potentials admit a Floquet space-harmonic representation [42, 22] imposed by the trace-velocity matching principle. The reflected acoustic potential ϕ_r reads

$$\phi_r = \sum_{s=-\infty}^{+\infty} R_s \mathrm{e}^{\mathrm{i}\alpha_s z}\mathrm{e}^{\mathrm{i}k_s^- x}, \quad x \le 0 \tag{9}$$

with

$$\alpha_s = \alpha_i + s\frac{2\pi}{a}, \quad k_s^- = \frac{-Mk - \overline{k_s}}{\beta^2}, \quad \overline{k_s} = \sqrt{k^2 - \beta^2\alpha_s^2}.$$

Similarly the transmitted acoustic potential ϕ_t is written as

$$\phi_t = \sum_{s=-\infty}^{+\infty} T_s \mathrm{e}^{\mathrm{i}\alpha_s z}\mathrm{e}^{\mathrm{i}k_s^+(x-c)}, \quad c \le x\ , \tag{10}$$

with $k_s^+ = [-Mk + \overline{k_s}]/\beta^2$. $\mathbf{R} = [R_s]$ and $\mathbf{T} = [T_s]$ are the corresponding vectors of unknown, complex-valued modal coefficients in Eqs. (9) and (10).

The upstream ϕ_u^m and downstream ϕ_d^m acoustic potentials in the m^{th} inter-vane channel can be written as

$$\begin{pmatrix} \phi_d^m \\ \phi_u^m \end{pmatrix} = \sum_{q=0}^{+\infty} \begin{pmatrix} D_q^0 \\ U_q^0 \end{pmatrix} e^{imu} \cos\Big(\alpha_q(z - ma)\Big) \begin{pmatrix} e^{ik_q^+ x} \\ e^{ik_q^-(x-c)} \end{pmatrix}, \qquad 0 \le x \le c \tag{11}$$

with

$$\alpha_q = \frac{q\pi}{a}, \quad k_q^{\pm} = \frac{-Mk \pm \overline{k_q}}{\beta^2}, \quad \overline{k_q} = \sqrt{k^2 - \beta^2 \alpha_q^2}.$$

ϕ_q^0 and D_q^0 stand for the modal coefficients in the reference channel (m=0). Indeed, adjacent inter-vane channels are phase-shifted by e^{iu} with $u = \alpha_i a = 2\pi n/V$, so that for instance $U_q^m = U_q^0 e^{imu}$ is the coefficient in the channel of index m. By virtue of the vane-to-vane phase-shift, the problem of the determination of the acoustic potentials only needs to be solved for the reference channel of index 0. Therefore $\mathbf{D}^0 = \left[D_q^0\right]$ and $\mathbf{U}^0 = \left[U_q^0\right]$ are the only vectors of modal coefficients to be determined in Eq. (11).

3.2. Matching equations

The continuity of the fluctuating pressure and axial velocity is imposed on both interfaces of the stator. Consequently two sets of matching equations are written at $x = 0$ and $x = c$. For clarity, a vector $\boldsymbol{\Gamma}_\gamma$ gathering all pressure and axial-velocity waves is considered. The index γ stands either for the incident (i), reflected (r) or transmitted (t) waves, or for the downstream (d) and upstream (u) acoustic (ac) waves in the channel:

$$\boldsymbol{\Gamma}_\gamma(x, z) = \begin{pmatrix} p_\gamma^{ac}(x, z) \\ \mathbf{v}_\gamma^{ac}(x, z) \cdot \mathbf{e}_x \end{pmatrix}, \quad \gamma = i, r, t, d, u.$$

The matching equations read:

$$\boldsymbol{\Gamma}_i(0, z) + \boldsymbol{\Gamma}_r(0, z) = \boldsymbol{\Gamma}_d(0, z) + \boldsymbol{\Gamma}_u(0, z), \quad \forall z, \tag{12}$$

$$\boldsymbol{\Gamma}_d(c, z) + \boldsymbol{\Gamma}_u(c, z) = \boldsymbol{\Gamma}_t(c, z), \quad \forall z. \tag{13}$$

These equations involve four unknown generic variables ($\mathbf{R}$, $\mathbf{D}^0$, $\mathbf{U}^0$, $\mathbf{T}$). A global matrix inversion method could be used with a proper truncation but it might not be the best suited because of conditioning issues. Furthermore considering each interface separately might have an interest for the understanding of the multiple scattering. This is why a different procedure is chosen, described in the next section.

3.3. Solving procedure

3.3.1. Iterative alternate matching

The two sets of Eqs. (12) and (13) can be solved by an iterative procedure which follows the onset of multiple scattered waves through the stator. The incident wave impinging on the leading-edge interface generates primary reflected waves upstream and transmitted waves downstream inside the reference channel, of acoustic potentials ϕ_r and ϕ_d^0 The transmitted waves are scattered at the trailing-edge interface, generating secondary upstream-reflected guided waves of potential ϕ_u^0 and the transmitted field ϕ_t downstream of the stator, and so on. Back-and-forth acoustic waves develop this way in the bifurcated waveguides until convergence. Let the iterations of the solving algorithm be numbered by the integer g.

In the initialization step ($g = 0$), Eq. (12) is solved without upstream wave in the channels (vector $\mathbf{U}^0 = \mathbf{0}$) and the calculated transmitted waves ($\mathbf{D}^0$) are used to solve Eq. (13). In fact the equations reduce to the system

$$\boldsymbol{\Gamma}_i(0, z) + \boldsymbol{\Gamma}_r^0(0, z) = \boldsymbol{\Gamma}_d^0(0, z), \quad \forall z, \tag{14}$$

$$\boldsymbol{\Gamma}_d^0(c, z) + \boldsymbol{\Gamma}_u^0(c, z) = \boldsymbol{\Gamma}_t^0(c, z), \quad \forall z. \tag{15}$$

and provide an initial value for all scattered waves. For the next iteration Eq. (12) is solved again using the modal coefficients from the upstream channel wave (vector $\mathbf{U}^0$) as input. The alternate iteration of any order $g > 0$ corresponds to the system

$$\boldsymbol{\Gamma}_i(0, z) + \boldsymbol{\Gamma}_r^g(0, z) = \boldsymbol{\Gamma}_d^g(0, z) + \boldsymbol{\Gamma}_u^{g-1}(0, z), \quad \forall z, \tag{16}$$

$$\boldsymbol{\Gamma}_d^g(c, z) + \boldsymbol{\Gamma}_u^g(c, z) = \boldsymbol{\Gamma}_t^g(c, z), \quad \forall z. \tag{17}$$

The process is continued until all coefficients $\mathbf{R}$, $\mathbf{D}^0$, $\mathbf{U}^0$ and $\mathbf{T}$ are converged. The convergence is ensured when the modal coefficients vary by less than 0.1% between two consecutive iterations (in practice, it is achieved after a few iterations). At every step in this procedure, only two vectors of coefficients ($\mathbf{R}$, $\mathbf{D}^0$) or ($\mathbf{U}^0$, $\mathbf{T}$) have to be determined for each interface, which makes the system of Eqs. (12) and (13) easily solved.

3.3.2. Modal projection

A usual way of solving the matching equations is to perform modal projections. This procedure, based on the orthogonality properties of the normal modes, leads to an infinite system of linear equations for the unknown modal coefficients. It is illustrated here for the trailing-edge interface because the latter will be re-addressed in the next section dealing with the Kutta condition. A similar statement would hold for the leading-edge interface. The matching at $x = c$ and for the reference channel ($m = 0$) produces the following set of equations for the acoustic pressure and axial velocity:

- continuity of pressure

$$\sum_{q=0}^{+\infty} (k - k_q^+ M) D_q^0 \cos\left(\alpha_q z\right) e^{ik_q^+ c} + (k - k_q^- M) U_q^0 \cos\left(\alpha_q z\right) = \sum_{s=-\infty}^{+\infty} (k - k_s^+ M) T_s e^{i\alpha_s z}, \tag{18}$$

- continuity of axial velocity

$$\sum_{q=0}^{+\infty} ik_q^+ D_q^0 \cos\left(\alpha_q z\right) e^{ik_q^+ c} + ik_q^- U_q^0 \cos\left(\alpha_q z\right) = \sum_{s=-\infty}^{+\infty} ik_s^+ T_s e^{i\alpha_s z}. \tag{19}$$

The system of Eqs. (18) and (19) is reduced using the following modal projection:

$$\int_0^a e^{-i\alpha_\mu z}(\bullet) dz \quad \text{with} \quad \alpha_\mu = \alpha_i + \mu \frac{2\pi}{a}, \quad \mu \in \mathbb{Z}, \tag{20}$$

leading to:

$$\sum_{q=0}^{+\infty} (k - k_q^+ M) \varphi_{\mu,q} D_q^0 e^{ik_q^+ c} + (k - k_q^- M) \varphi_{\mu,q} U_q^0 = (k - k_\mu^+ M) T_\mu a, \tag{21}$$

$$\sum_{q=0}^{+\infty} ik_q^+ \varphi_{\mu,q} D_q^0 e^{ik_q^+ c} + ik_q^- \varphi_{\mu,q} U_q^0 = ik_\mu^+ T_\mu a, \tag{22}$$

where

$$\begin{aligned} \varphi_{\mu,q} &= \frac{i\alpha_\mu\left(1 - (-1)^q e^{-iu}\right)}{\alpha_q^2 - \alpha_\mu^2}, \quad \text{if} \quad \alpha_\mu \neq \pm \alpha_q, \\ \varphi_{\mu,q} &= \frac{a}{2}(1 + \delta_{q,0}), \quad \text{if} \quad \alpha_\mu = \pm \alpha_q, \end{aligned}$$

and where $\delta_{q,0}$ stands for the Kronecker symbol. Truncating the infinite sums to N_q channel modes and to $2N_s + 1$ transmitted modes, Eqs. (21) and (22) can be written in a matrix form as:

$$\begin{pmatrix} \underline{\mathbf{E}}_p & \underline{\mathbf{F}}_p \\ \underline{\mathbf{E}}_v & \underline{\mathbf{F}}_v \end{pmatrix} \begin{pmatrix} \mathbf{U}^0 \\ \mathbf{T} \end{pmatrix} = \begin{pmatrix} \mathbf{H}_p \\ \mathbf{H}_v \end{pmatrix} \tag{23}$$

with

$$\begin{aligned} E_p(\mu, q) &= (k - k_q^- M) \varphi_{\mu,q} & E_v(\mu, q) &= ik_q^- \varphi_{\mu,q} \\ F_p(\mu, \mu) &= -a(k - k_\mu^+ M) & F_v(\mu, \mu) &= -iak_\mu^+ \\ H_p(\mu, 1) &= -\sum_{q=0}^{N_q - 1} (k - k_q^+ M) \varphi_{\mu,q} D_q^0 e^{ik_q^+ c} & H_v(\mu, 1) &= -\sum_{q=0}^{N_q - 1} ik_q^+ \varphi_{\mu,q} D_q^0 e^{ik_q^+ c} \end{aligned}$$

Though a pseudo-inverse could also be used, the same number of channel and transmitted modes is chosen to obtain a square linear system. $\mathbf{D}^0$ is calculated by the initialization step of the iterative method, Eq. (14). The associated matrix, being well-conditioned, is inversed so that the vectors of modal coefficients $\mathbf{U}^0$ and $\mathbf{T}$ are computed. Alternatively, closed-form expressions could be derived for the modal coefficients using a residue-calculus method, as pointed by Ingenito and Roger [33]. This has not been attempted here because the expressions would be very cumbersome for the coupling of two interfaces, on the one hand, and because the equations will be completed with a Kutta condition for which the explicit derivation of the coefficients is not achievable anymore, on the other hand.

3.4. Formulation including a Kutta condition

First considerations on the Kutta condition for the sound diffraction by the trailing edge of a half-plane immersed in a mean flow were provided by Jones [43]. Addressed in a two-dimensional configuration, the solution of the diffraction problem must satisfy the convected Helmholtz equation, the rigid-wall boundary condition and the Sommerfeld radiation condition, the field being continuous with a finite local energy. Jones proved that this solution is unique but has an infinite velocity at the trailing-edge because of the inviscid-fluid assumption. The Kutta condition (as in airfoil theory) enforces a finite velocity at the trailing-edge. According to Rienstra [44], this condition is also equivalent to impose a zero-pressure jump at the edge. Finding a solution requires introducing a shed vorticity in the continuation of the half-plane. The shed vorticity is assumed to be an infinitely thin oscillating vortex sheet convected by the mean flow because of its hydrodynamic nature. Although the vortex sheet is acoustically quiet, in the sense that no pressure perturbation is associated with it, the sound field significantly depends on whether the Kutta condition is imposed or not, which has been recognized by many authors (Jones [43], Rienstra [44], Howe [45], Job [46]). The condition is imposed here for physical consistency.

3.4.1. Additional equations

When applied at the trailing edges of the vanes in the mode-matching formulation, the Kutta condition imposes a zero pressure jump between both sides of a vane in adjacent channels as x approaches c from upstream. Farther downstream the continuity of the pressure is ensured by the modal expression of the transmitted field. Considering the reference channel, the condition produces a new equation for the vector $\mathbf{U}^0$:

$$\sum_{q=0}^{N_q-1}(1-(-1)^q\mathrm{e}^{-\mathrm{i}u})(k-k_q^-M)U_q^0=-\sum_{q=0}^{N_q-1}(1-(-1)^q\mathrm{e}^{-\mathrm{i}u})(k-k_q^+M)D_q^0\mathrm{e}^{\mathrm{i}k_q^+c}. \quad (24)$$

Solving the matching equations (Eq. (23)) with the Kutta condition (Eq. (24)) would lead to an over-determined linear system. An approximate solution could be found using a least-square minimization approach but this would not be rigorous anymore.

In a two-dimensional approach, Howe [45] suggests that the vorticity generated by the Kutta condition can be concentrated on lines at $z=ma$, $c\le x$, assuming that the associated hydrodynamic wavelength is large compared to the vane and wake thicknesses (see Fig. 4). This assumption is relevant when modeling the vanes as zero-thickness plates. Consequently, the vorticity field can be modeled as a Dirac comb, the Dirac functions of adjacent trailing edges being phase-shifted. The vorticity waves are simply convected by the mean flow. Their expression is given as:

$$\mathbf{\Omega}_K(x,z)=\Omega_0\mathrm{e}^{\mathrm{i}(\omega/W_x)(x-c)}\sum_{m=-\infty}^{+\infty}\mathrm{e}^{\mathrm{i}mu}\delta(z-ma)\mathbf{e}_y,\quad u=a\alpha_i=\frac{2\pi n}{V},\quad c\le x. \quad (25)$$

Ω_0 represents the magnitude of the vorticity and is a new unknown variable. Physically, it represents the amount of shed vorticity introduced to cancel the singularity at the edge. The Dirac comb of vorticity can be expanded into a Fourier series. As a result, the vorticity field is written as an infinite sum of oblique gusts. The vorticity vector reads

$$\mathbf{\Omega}_K(x,z)=\frac{\Omega_0}{a}\sum_{s=-\infty}^{+\infty}\mathrm{e}^{\mathrm{i}(\omega/W_x)(x-c)}\mathrm{e}^{\mathrm{i}\alpha_s z}\mathbf{e}_y,\quad \alpha_s=\alpha_i+s\frac{2\pi}{a},\quad c\le x. \quad (26)$$

and the associated velocity field $\mathbf{v}_K^h$ also admits a plane-wave expansion. The definition of the vorticity, $\mathbf{\Omega}_K=\nabla\times\mathbf{v}_K^h$ and the incompressibility of the velocity field ($\nabla\cdot\mathbf{v}_K^h=0$) determine each velocity component. The expression for the axial velocity is obtained as:

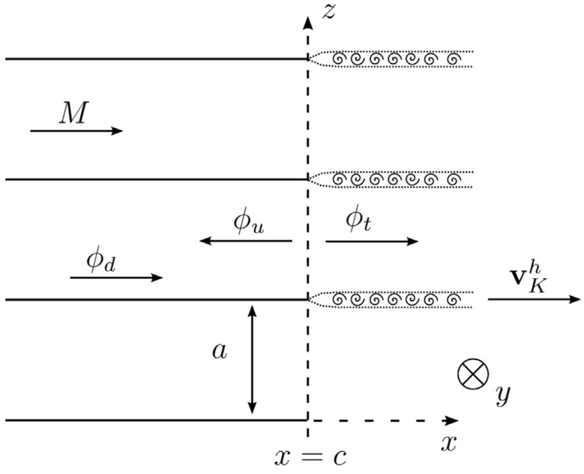

Fig. 4. Modeling of the vorticity perturbations induced by the Kutta condition downstream of the vanes (according to Howe [45]).

$$\mathbf{v}_K^h \cdot \mathbf{e}_x = \sum_{s=-\infty}^{+\infty} V_s \mathrm{e}^{\mathrm{i}(\omega/W_x)(x-c)} \mathrm{e}^{\mathrm{i}\alpha_s z}, \quad V_s = \frac{\mathrm{i}\Omega_0 \alpha_s}{a\left(\alpha_s^2 + (\omega/W_x)^2\right)}, \quad c \le x. \tag{27}$$

This hydrodynamic velocity component must be included into the matching equation for the axial velocity at the trailing-edge interface. Using the scalar product from Eq. (20) leads to:

$$\sum_{q=0}^{+\infty} \mathrm{i}k_q^+ \varphi_{\mu,q} D_q^0 \mathrm{e}^{\mathrm{i}k_q^+ c} + \mathrm{i}k_q^- \varphi_{\mu,q} U_q^0 = \mathrm{i}k_\mu^+ T_\mu a + \mathrm{i}\frac{\alpha_\mu}{\alpha_\mu^2 + (\omega/W_x)^2}\Omega_0, \quad \mu \in \mathbb{Z}. \tag{28}$$

3.4.2. Completed solving procedure

The hydrodynamic velocity fluctuations being pressure-free, the matching equation for the pressure (Eq. (21)) remains unchanged when the Kutta condition is active. Choosing the same number of channel and transmitted modes enables to build again a square linear system with the matching equations (Eqs. (21) and (28)) and the Kutta condition (Eq. (24)). The new matrix form reads:

$$\begin{pmatrix} \underline{\mathbf{E}}_p & \underline{\mathbf{F}}_p & \mathbf{0} \\ \underline{\mathbf{E}}_v & \underline{\mathbf{F}}_v & \mathbf{G}_v^K \\ \mathbf{E}_K & \mathbf{0} & 0 \end{pmatrix} \begin{pmatrix} \mathbf{U}^0 \\ \mathbf{T} \\ \Omega_0 \end{pmatrix} = \begin{pmatrix} \mathbf{H}_p \\ \mathbf{H}_v \\ H_K \end{pmatrix} \tag{29}$$

with

$$E_K(1, q) = (k - k_q^- M)(1 - (-1)^q \mathrm{e}^{-\mathrm{i}u}) \qquad G_v^K(\mu, 1) = \mathrm{i}\frac{\alpha_\mu}{\alpha_\mu^2 + (\omega/W_x)^2}$$

$$H_K(1, 1) = -\sum_{q=0}^{N_q-1} \mathrm{e}^{\mathrm{i}k_q^+ c}(1 - (-1)^q \mathrm{e}^{-\mathrm{i}u})(k - k_q^+ M) D_q^0$$

The elementary matrices $\underline{\mathbf{E}}_p$, $\underline{\mathbf{E}}_v$, $\underline{\mathbf{F}}_p$, $\underline{\mathbf{F}}_v$ and vectors $\mathbf{H}_p$, $\mathbf{H}_v$ remain unchanged. This linear system is well conditioned and solved by matrix inversion.

In the following sections, the mode-matching technique will always refer to the formulation including the Kutta condition, unless otherwise mentioned.

3.5. Validation and sample results

The mode-matching technique is applied in this section to an oblique plane wave incident from upstream on a two-dimensional cascade. The main parameters are the wave angle of incidence $\Theta = 30°$, the chord-based Helmholtz number $k \times c = 5$ and the solidity $\sigma = c/a = 1.25$. They are chosen in accordance with the test-case solved with the Wiener-Hopf technique in references [47,48] to allow the comparison between the approaches. In practical turbomachinery applications, these parameters would be tuned to reproduce the 2π-periodicity of the original stator. In each case, the instantaneous acoustic pressure is normalized by the incident acoustic pressure $p_i = -\mathrm{i}\rho_0 c_0 (k - k_i^+ M)$.

3.5.1. Sample results

Fig. 5-a presents the instantaneous pressure resulting from the scattering of the oblique acoustic wave at $M = 0.2$ A very good overall continuity of the field is found. The associated modal amplitudes are displayed in Fig. 5-b. In the domains upstream and downstream of the vanes, only the mode of scattering order $s = 0$ is cut-on. As a result, the transmitted field is essentially a plane wave that propagates in the same direction as the incident wave. In the absence of mean flow, the reflected wave of scattering order 0 would propagate in the upstream direction with an angle of propagation $\Theta_r = -\Theta$ (Eq. (8)). However its axial group velocity is reduced by the composition with the mean-flow velocity. Therefore, it has an increased angle ($|\Theta_r| > |\Theta|$). The modal amplitudes of the cut-on waves also show that more energy from the incident wave is transferred into the transmitted wave than into the reflected wave.

Fig. 5-b also displays the modal amplitudes in the channels, highlighting that the modes $q = 0$ and $q = 1$ are cut-on. For the waves propagating downstream, the plane-wave mode $q = 0$ dominates. Nevertheless, the mode $q = 1$ has a significant amplitude. Its structure exhibits opposite phases on the lower and upper boundaries of the channels. For the modes propagating upstream, the acoustic energy is balanced differently in such a way that the mode $q = 1$ is now dominant.

3.5.2. Comparison with the Wiener-Hopf technique

As mentioned in the introduction the problem of wave-scattering by a rectilinear cascade of vanes can be solved alternatively using the Wiener-Hopf technique. The extension of Glegg's model [16] by Posson et al. [17] provides a uniformly valid description of the acoustic field in the whole space. It has been successfully compared with other rectilinear cascade models both in terms of unsteady loading on the vanes and of pressure fields in the inter-vane channels. Consequently, as a first step in the validation process, the results obtained with the Wiener-Hopf technique and with the present mode-

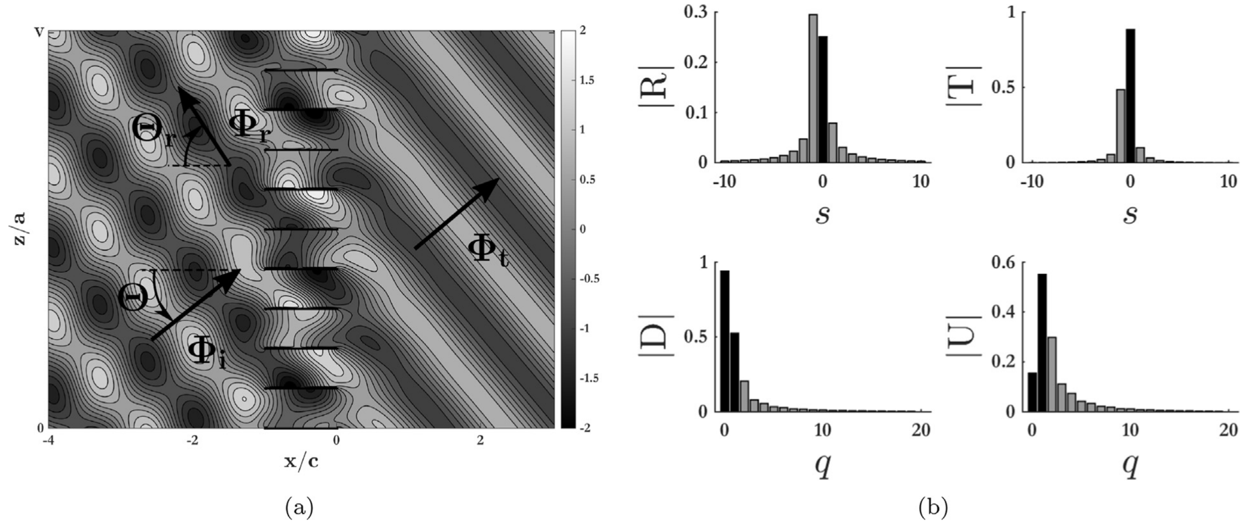

Fig. 5. (a): Normalized instantaneous acoustic pressure field obtained with the mode-matching technique for $M = 0.2$. (b): Modulus of the modal reflection (**R**), transmission (**T**) and channel ($\mathbf{D}^0$, $\mathbf{U}^0$) wave coefficients. Black and gray bars denote cut-on and cut-off modes respectively. The flow goes from left to right.

matching technique are compared in this section.

Fig. 6 presents the normalized instantaneous acoustic pressure fields obtained with the mode matching for the same incident wave and various Mach numbers. Identical acoustic pressure fields are obtained with the Wiener-Hopf technique. The effect of the Mach number is significant: the adjacent wave fronts of the downstream propagating waves are stretched by convection whereas those of the upstream waves are contracted. This is responsible for the wiggles appearing in the left part of the maps, more pronounced at $M = 0.6$ and $M = 0.8$. Furthermore, with increasing Mach number, additional modes become cut-on because of the effect of the compressibility factor β. For instance, two modes propagate downstream and upstream of the vanes at $M = 0.6$ and $M = 0.8$ whereas only one does at $M = 0.2$ and $M = 0.4$.

A full agreement has been found at any subsonic Mach number between the Wiener-Hopf technique and the mode-matching technique, which confirms that the implementation of the latter is reliable in terms of convergence and truncation. This is confirmed in a more quantitative way by plotting instantaneous pressure profiles along an axial line at the center of the channels according to both formulations, in Fig. 7, and the real part of the normalized unsteady pressure jump across a reference vane (at $z/a = 1$) $\mathcal{L} = -\Delta p/(\mathrm{i}\rho_0 c_0(k - k_i^+ M))$, in Fig. 8. Both sets of results are in an almost perfect agreement. Slight discrepancies are only noticed on the normalized unsteady pressure jump in the very vicinity of the leading edge, where the mode-matching exhibits a singularity. The latter has no consequence away from the leading edge.

Fig. 7 also illustrates the effect of the Kutta condition in the mode-matching formulation. When this condition is not considered (grey profiles in the figure), the predictions strongly deviate from the Wiener-Hopf results which account for it. The magnitudes of the reflected and transmitted waves are significantly overestimated. The discrepancies have been found to be dramatically increased with increasing Mach number. Therefore the Kutta condition appears as essential in the mathematical modeling.

4. Scattering of a vortical gust

The scattering of vortical waves by a cascade into sound is the second generic problem addressed here (Fig. 9), in connection with the modeling of rotor-stator wake interaction noise in a turbomachinery context.

The theoretical background is inherited from Chu and Kovásznay [49] who showed that a gas can experience three kinds of oscillatory motion referred to as the acoustic, vortical and entropy modes. The present analysis is restricted to the acoustic and vortical modes, assuming that the entropy is constant and uniform. The acoustic mode corresponds to compressible, irrotational and propagating perturbations, whereas the vortical mode corresponds to incompressible, divergence-free perturbations which are convected by the mean-flow. These oscillating motions remain uncoupled within the scope of a linearized analysis (limit of very small perturbations) provided that the base flow is homogeneous and unbounded. As a consequence, each mode can exist independently and be described without taking the other two into account. However, the modes are theoretically coupled at physical boundaries. In the case of a wake impingement on a cascade of OGV this occurs here at the walls of the inter-vane channels where the sum of the acoustic and vortical normal velocities has to go to zero. Yet a different but equivalent standpoint is taken in the mode-matching technique. The vortical excitation is first prescribed as a purely frozen and convected pattern in the whole domain independently of the cascade and of the acoustic motion. The latter is defined as the response of the cascade, such that the rigid-wall boundary condition on the vanes is fulfilled. Instead

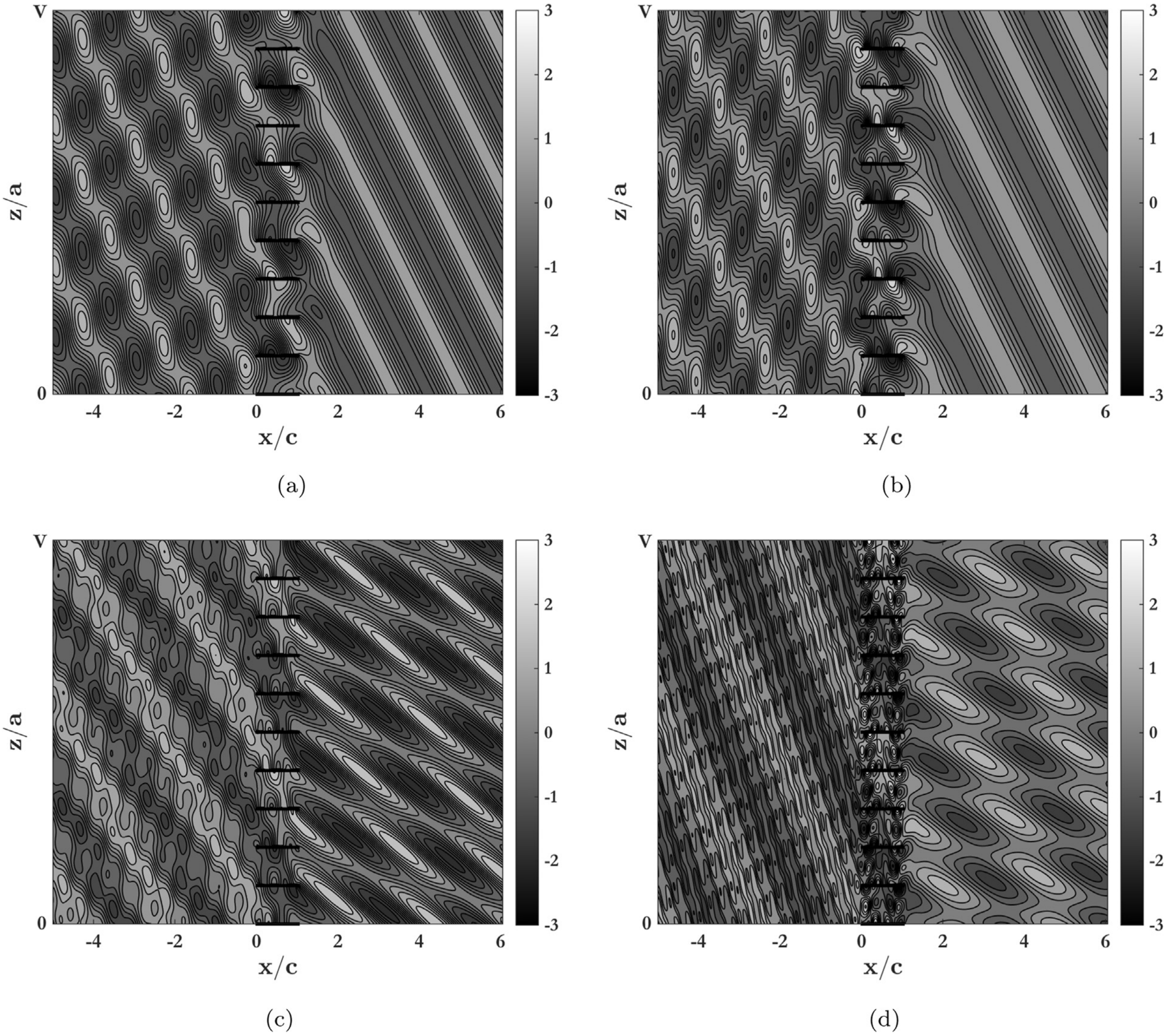

Fig. 6. Normalized instantaneous acoustic pressure fields obtained indifferently with the Wiener-Hopf technique and the mode-matching technique for $M = 0.2$ (a), $M = 0.4$ (b), $M = 0.6$ (c) and $M = 0.8$ (d). The flow goes from left to right.

of using this condition directly, the vortical and acoustic fields are both expressed as sums of modes inside the channels so that they automatically satisfy it. The connection between the vortical and acoustic motions is displaced from the walls to the matching interface, where it is achieved by writing local continuity conditions. Because the fundamental gas-dynamics equations and the boundary conditions are satisfied anyway, the mathematical statement is as exact as with alternative formulations.

4.1. Wake modeling

4.1.1. Incident wakes

The mode-matching technique applied to wake interactions first requires the description of the periodic velocity deficit in the rotor wakes and its expansion in vortical gusts impinging on the stator. At the preliminary design stage of a rotor/stator system, a numerical computation may not be available to provide information about the wakes. Therefore a suitable alternative consists in assimilating the wake velocity deficit to a Gaussian function, the parameters of which are tuned from inspection of the rotor blade geometry, its stagger angle and the distance between the trailing edges of the blades and the leading edges of the stator vanes. The reliability of the approach has been reported by Roger [50]. The Gaussian shape of the velocity deficit profile along the wake used in the present study was proposed by Reynolds et al. [51]. The periodic wake-velocity deficit for a rotor with B identical and equally spaced blades as seen from a fixed location is expressed by repeating the wake profile as an infinite series of time Gaussian pulses:

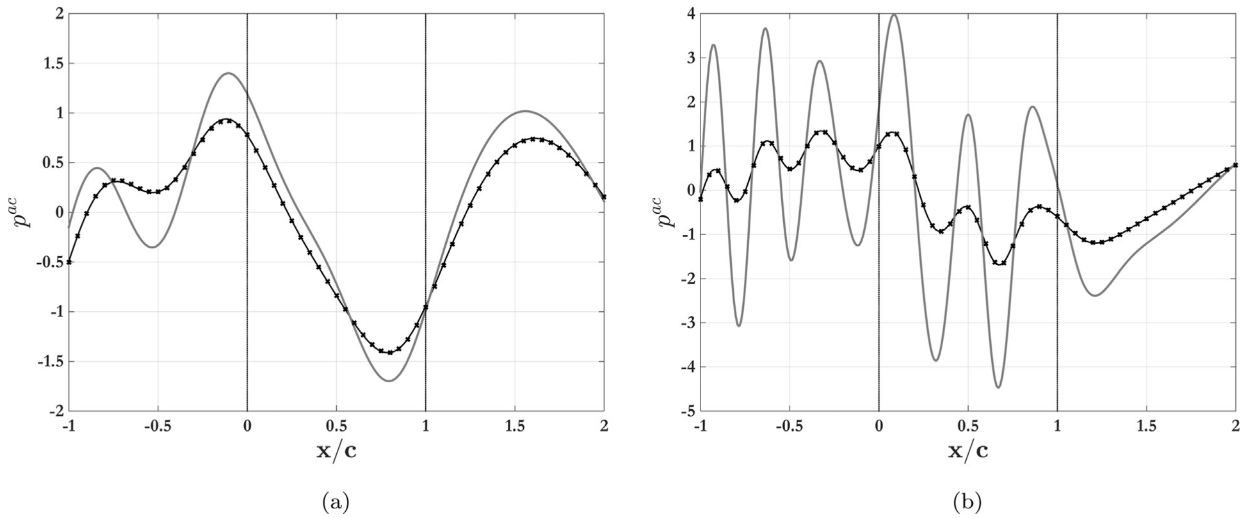

Fig. 7. Profiles of normalized instantaneous acoustic pressure in the streamwise direction at $z/a = 0.5$ (center of the channel) at $M = 0.4$ (a) and $M = 0.4$ (b), obtained with the Wiener-Hopf technique (black symbols), the mode-matching technique (black plain line) and the mode-matching technique without the Kutta condition (gray line).

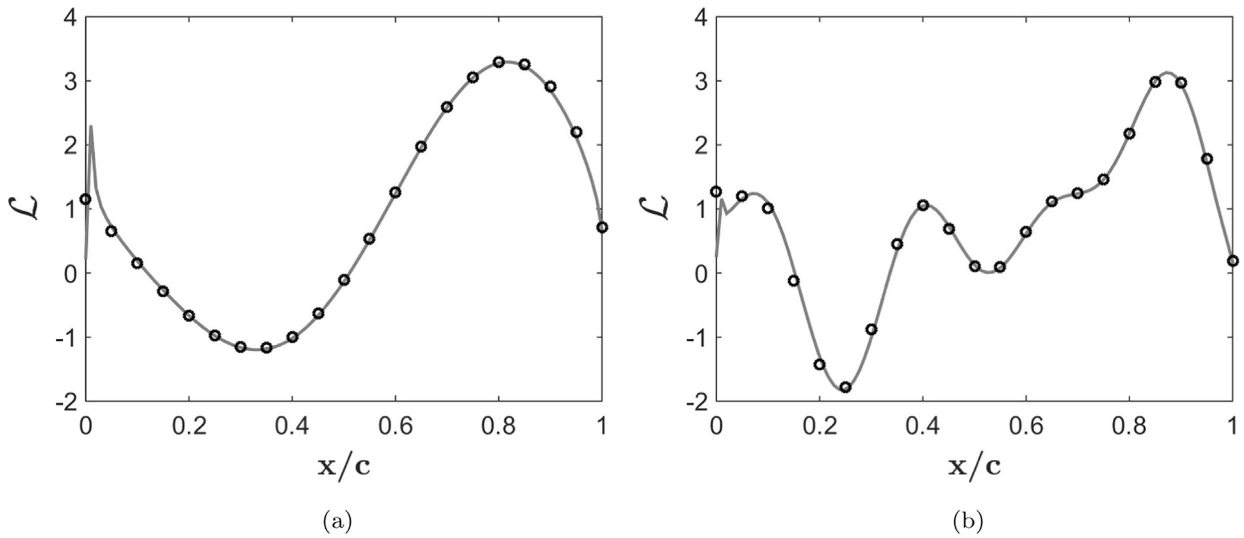

Fig. 8. Real part of the normalized pressure jump on a vane for $M = 0.4$ (a) and $M = 0.8$ (b) as predicted by the mode matching (plain line) and the Wiener-Hopf technique (symbols).

$$w(t) = w_0 \sum_{k=-\infty}^{+\infty} \mathrm{e}^{-\xi\left(\frac{t-kT}{\tau}\right)^2} = \sum_{n=-\infty}^{+\infty} w_n \mathrm{e}^{-\mathrm{i}nB\Omega t}, \tag{30}$$

where

$$w_n = \frac{w_0 Bb}{2\pi R_0}\sqrt{\frac{\pi}{\xi}}\,\mathrm{e}^{-(nBb)^2/(4\xi R_0^2)}.$$

Here $\xi = \ln 2$, w_0 is the velocity deficit on the wake centerline, $\tau = b/(\Omega R_0)$ is half the characteristic time of the impulse corresponding to a single wake passage, b is the half-width of the wake profile and T is the wake passing period corresponding to the wake passing frequency $B\Omega/(2\pi)$. The associated angular Blade Passing Frequencies (BPF) are $\omega_n = nB\Omega$. The spectrum of the wake harmonics decreases with a Gaussian envelope. Furthermore, accounting for the convection, the axial projection of the wake velocity deficit at a fixed time in the stator reference frame follows as

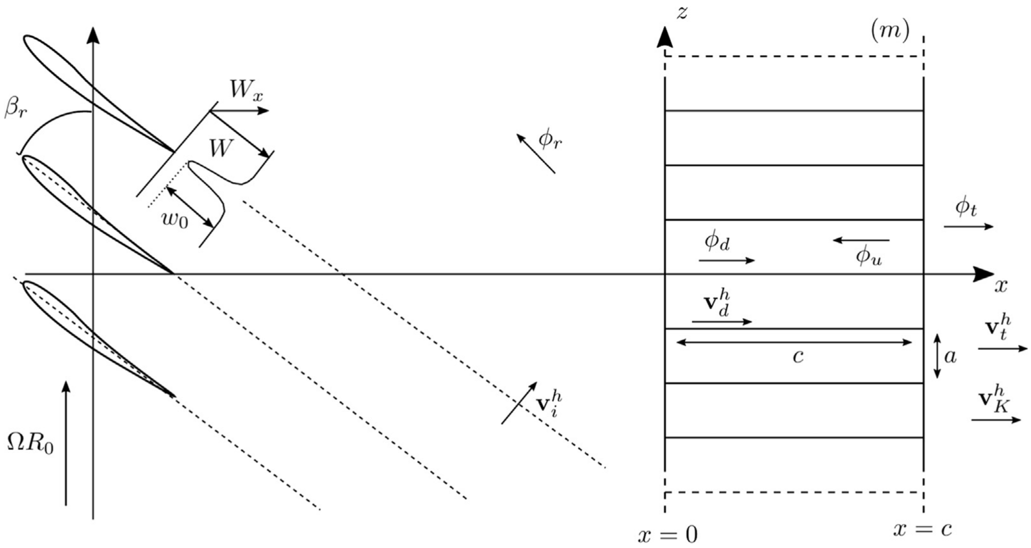

Fig. 9. Wake impingement on a cascade of OGV. 2D unwrapped representation, main notations and conventions.

$$\mathbf{v}_i^h \cdot \mathbf{e}_x = \sin(\beta_r) \sum_{n=-\infty}^{+\infty} w_n e^{i\alpha_n z} e^{ik_n^+ x}, \quad x \leq 0, \quad n \neq 0. \tag{31}$$

with

$$\alpha_n = \frac{nB}{R_0}, \quad k_n^+ = \frac{nB\Omega}{W_x}.$$

The term of order zero must be discarded since it contributes to the non-radiating steady loading on the vanes. Each contribution of order n produces sound at the corresponding multiple of the blade-passing frequency.

4.1.2. Wakes in the inter-vane channels

The continuation of a hydrodynamic gust inside the inter-vane channels must be specified in such a way that the axial convection by the flow, the rigid-wall condition on the vanes and the phase-shift between adjacent channels are preserved. For any value of n, the axial velocity of the gust in the bifurcated waveguides is written as a sum of modes:

$$\mathbf{v}_d^h \cdot \mathbf{e}_x = \sum_{q=1}^{+\infty} A_q^0 e^{imu} \cos\big(\alpha_q (z - ma)\big) e^{ik_n^+ x}, \quad \alpha_q = \frac{q\pi}{a}, \quad 0 \leq x \leq c. \tag{32}$$

The conservation of the rotational through the interfaces is expressed as:

$$\nabla \times \mathbf{v}_i^h = \nabla \times \mathbf{v}_d^h, \quad x = 0, \tag{33}$$

$$\nabla \times \mathbf{v}_d^h = \nabla \times \mathbf{v}_t^h, \quad x = c. \tag{34}$$

This conservation is used to define the modal amplitudes A_q^0 of the hydrodynamic gust in the reference channel. Moreover, the divergence of the hydrodynamic velocity field is zero, leading to a relationship between axial and azimuthal components.

Matching both expressions of the rotational at the leading-edge interface located at $x = 0$, the following equation is found:

$$i\left(\frac{\alpha_n^2 + (k_n^+)^2}{\alpha_n}\right) \sin(\beta_r) w_n e^{i\alpha_n z} = \sum_{q=1}^{+\infty} \left[\frac{\left(ik_n^+\right)^2}{\alpha_q} - \alpha_q\right] A_q^0 \sin\left(\alpha_q z\right). \tag{35}$$

Multiplying both sides by $\sin(\alpha_\mu z)$, $\alpha_\mu = \mu\pi/a$, $\mu \in \mathbb{Z}$, integrating with respect to z from 0 to a and taking advantage of the orthogonality of the modes leads to the infinite set of equations

$$i\left(\frac{\alpha_n^2 + (k_n^+)^2}{\alpha_n}\right) \sin(\beta_r) w_n \Psi_{\mu,n} = \left[\frac{\left(ik_n^+\right)^2}{\alpha_\mu} - \alpha_\mu\right] A_\mu^0 \frac{a}{2}, \quad \mu = 1, \ldots, N_\mu, \tag{36}$$

where

$$\Psi_{\mu,n} = \frac{\alpha_\mu[(-1)^\mu e^{iu} - 1]}{(\alpha_n^2 - \alpha_\mu^2)}, \quad \text{if} \quad \alpha_n \neq \alpha_\mu, \quad \Psi_{\mu,n} = \frac{ia}{2}, \quad \text{if} \quad \alpha_n = \alpha_\mu, \quad u = \alpha_n a.$$

Thus the modal amplitudes of the hydrodynamic modes in the channel are obtained as

$$A_\mu^0 = \frac{i\left(\dfrac{\alpha_n^2 + (k_n^+)^2}{\alpha_n}\right)\sin(\beta_r) w_n \Psi_{\mu,n}}{\left[\dfrac{(ik_n^+)^2}{\alpha_\mu} - \alpha_\mu\right]\dfrac{a}{2}}. \tag{37}$$

Finally the gust is assumed to be the same upstream and downstream of the cascade, so that its downstream expression is

$$\mathbf{v}_t^h \cdot \mathbf{e}_x = B_n e^{i\alpha_n z} e^{ik_n^+ x}, \quad \text{where} \quad B_n = \sin(\beta_r) w_n, \quad c \le x. \tag{38}$$

The relevance of this multiple definition of an incident gust is a key step in the mode-matching approach when modeling sound generating mechanisms. It will be checked in the Section 4.3.2.

4.1.3. Definition of the acoustic potentials

Four acoustic potential fields result from the interaction with the hydrodynamic gust, all solutions of the convected Helmholtz equation: the upstream-scattered and the downstream-scattered potentials in the free-field domains, still noted $\phi_r$and ϕ_t by similarity with the reflected and transmitted waves of the previous case, and those in the inter-vane channels again noted ϕ_u and ϕ_d with regard to their upstream or downstream direction of propagation. Though the modal form of those acoustic potential fields remains the same as for the diffraction of an acoustic plane wave on the stator, some quantities are modified in the case of the hydrodynamic gust impingement. Firstly, the azimuthal wavenumbers of the expressions of ϕ_r (Eq. (9)) and ϕ_t (Eq. (10)) become $\alpha_s = (nB + sV)/R_0$, $[n, s] \in \mathbb{Z}$. Secondly, the phase-shift between two adjacent channels is written as $u = 2\pi nB/V$. Finally, the wavenumber corresponding to the n^{th} multiple of the BPF is $k = k_n = nB\Omega/c_0$. It can be noted that the upstream-scattered and downstream-scattered fields result from the modulation of the incident perturbations by the periodicity of the V vanes, according to Tyler and Sofrin's rule [52].

4.2. Matching equations

For the impingement of a vortical wave, a new vector $\boldsymbol{\Gamma}_\gamma$ is considered, adding the vortical parts of the velocity field, induced by both the incident wake perturbations and the shed vorticity generated by the Kutta condition:

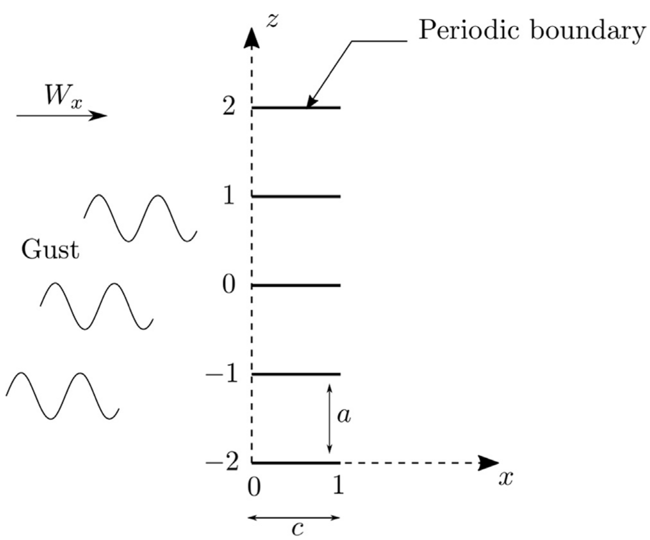

Fig. 10. Test-case definition, NASA Second CAA Workshop on Benchmark Problems Category 3 (1997) – Turbomachinery noise.

$$\boldsymbol{\Gamma}_{\gamma}(x,z)=\begin{pmatrix} p_{\gamma}^{ac}(x,z) \\ (\mathbf{v}_{\gamma}^{ac}(x,z)+\mathbf{v}_{\gamma}^{h}(x,z))\cdot\mathbf{e}_x \end{pmatrix},\quad \gamma=i,r,t,d,u. \tag{39}$$

The continuity of pressure and axial velocity is again imposed at the leading-edge interface ($x = 0$) and at the trailing-edge interface ($x = c$), leading to the same matching equations, Eqs. (12) and (13) solved by the method described in Section 3.3.

4.3. Validation

4.3.1. Definition of the test-case

The mode-matching solution for the scattering of a vortical wave by a two-dimensional cascade of vanes is tested in this section against the Category 3 benchmark problem defined in the NASA Second CAA Workshop on Benchmark Problems (Fig. 10). This test-case received contributions by Lockard and Morris [53] (parallel computing), Tam et al. [54] (Dispersion-

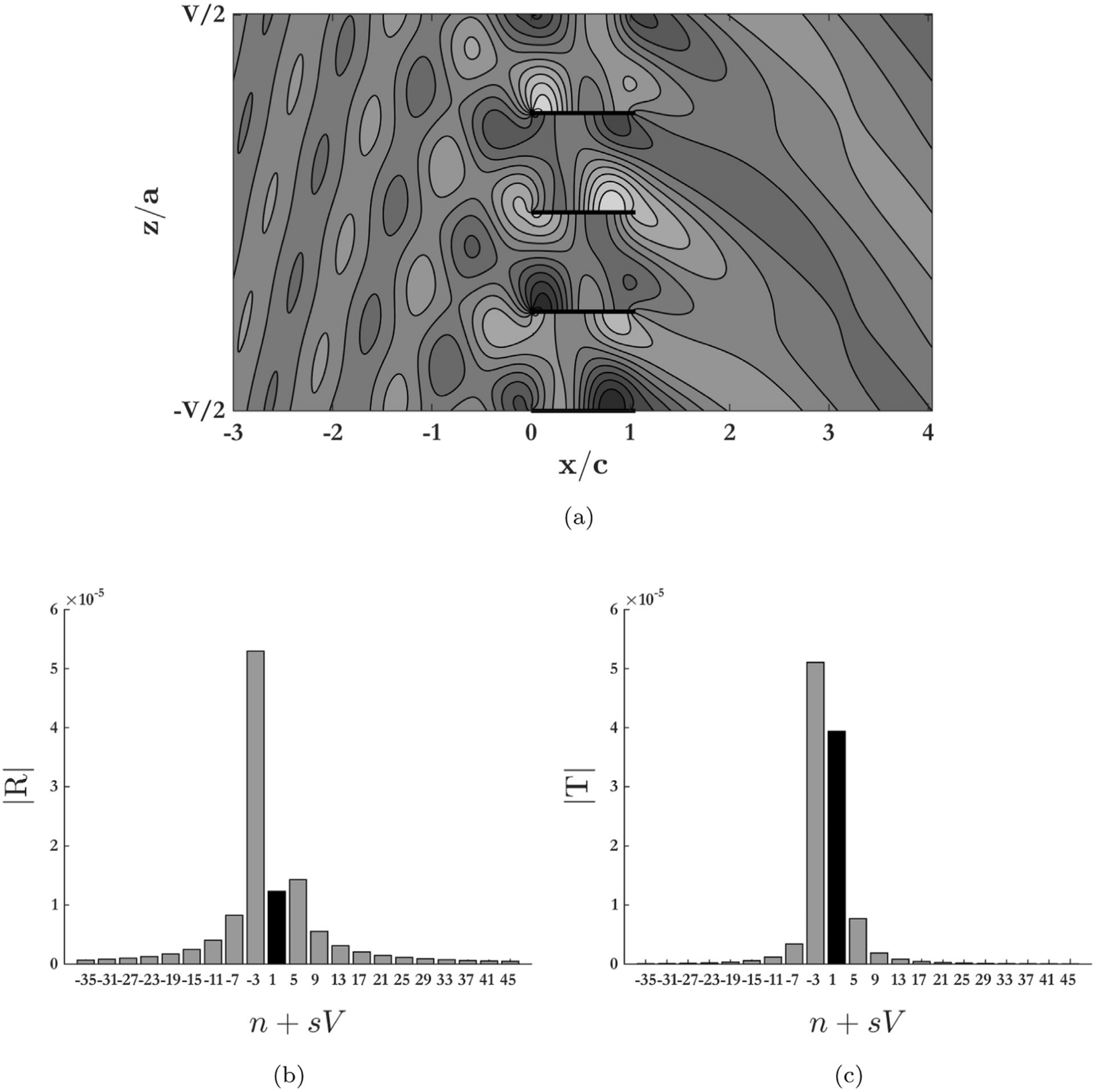

Fig. 11. Low-frequency test case of gust impingement on the front face of a cascade of vanes ($\overline{k_x} = 5\pi/2$). (a): Instantaneous pressure field. (b): Modal reflection $|\mathbf{R}|$ and (c): transmission $|\mathbf{T}|$ factors. Black and gray bars denote cut-on and cut-off modes respectively.

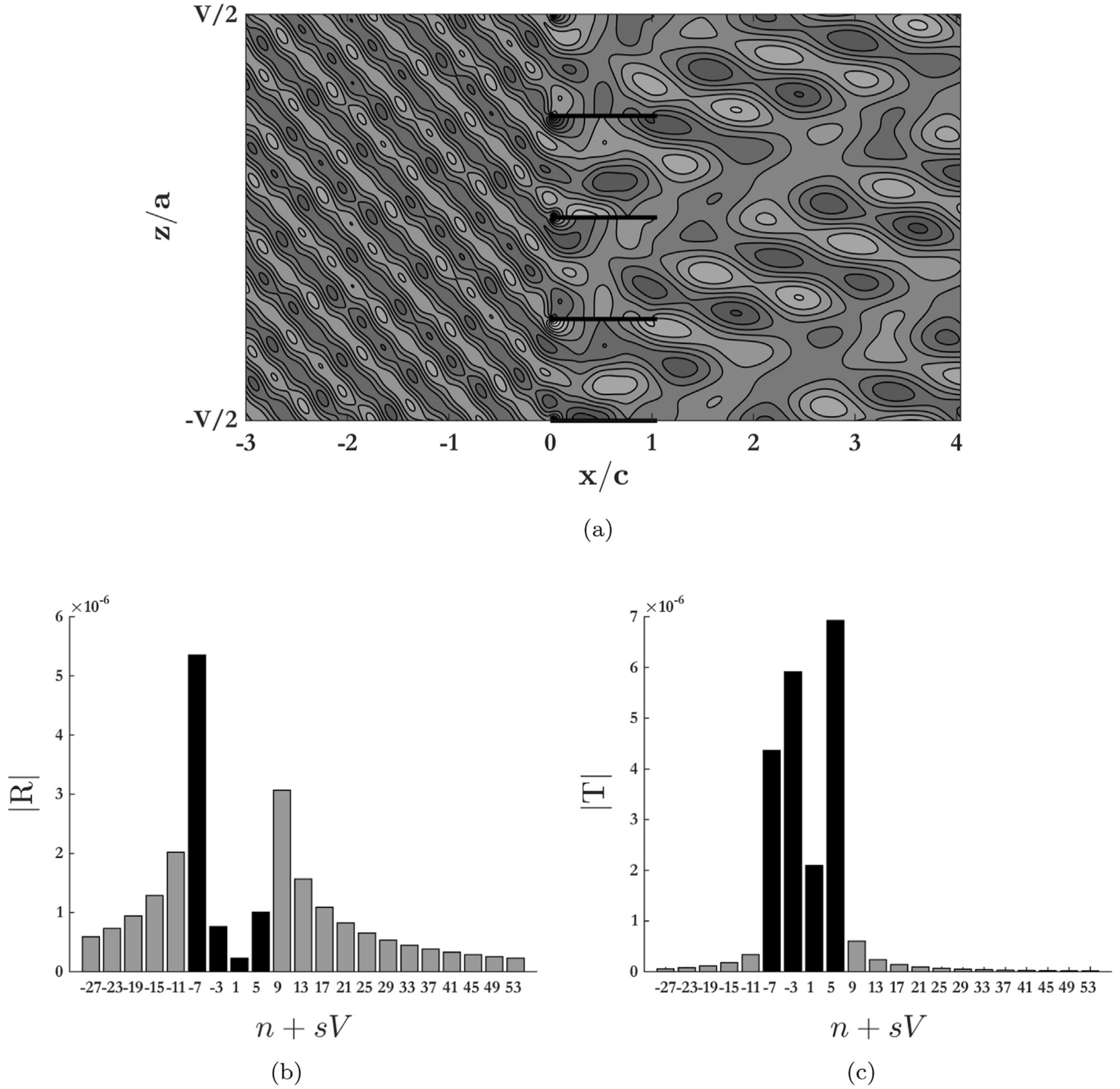

Fig. 12. High-frequency test case of gust impingement on the front face of a cascade of vanes ($\overline{k_x} = 13\pi/2$). (a): Instantaneous pressure field. (b): Modal reflection |**R**| and (c): transmission |**T**| factors. Black and gray bars denote cut-on and cut-off modes respectively.

Relation-Preserving (DRP) scheme), Hu and Manthey [55] (Perfectly Matched Layer (PML) application) and Hall [56,57], (variational finite-element method). This configuration was also used by Posson [47] to validate the analytical rectilinear-cascade model based on the Wiener-Hopf technique. More recently, Durand and Hixon [58] readdressed it using the NASA Glenn Research Center Broadband Aeroacoustic Stator Simulation (BASS) Computational Aeroacoustics (CAA) code. Fig. 10 illustrates the test-case cascade of flat-plate vanes ($V = 4$). The mean-flow is axial with a Mach number $M = W_x/c_0 = 0.5$. The solidity c/a is equal to 1. The incident vortical gust, convected by the mean-flow, is defined by its axial velocity:

$$\mathbf{v}_i^h(x, z) \cdot \mathbf{e}_x = w_0 \mathrm{e}^{\mathrm{i}(k_z z + k_x x - \omega t)}, \tag{40}$$

where $w_0 = 0.01$, $k_z = u/a$ and $k_x = \omega/W_x$. Variables are made dimensionless with respect to c as length scale and c/W_x as time scale. They are denoted with a bar so that Eq. (40) becomes

$$\mathbf{v}_i^h(x, z) \cdot \mathbf{e}_x = w_0 \mathrm{e}^{\mathrm{i}(u\bar{z} + \bar{k}_x \bar{x} - \bar{k}_x \bar{t})}, \quad \bar{k}_x = \frac{\omega c}{W_x}. \tag{41}$$

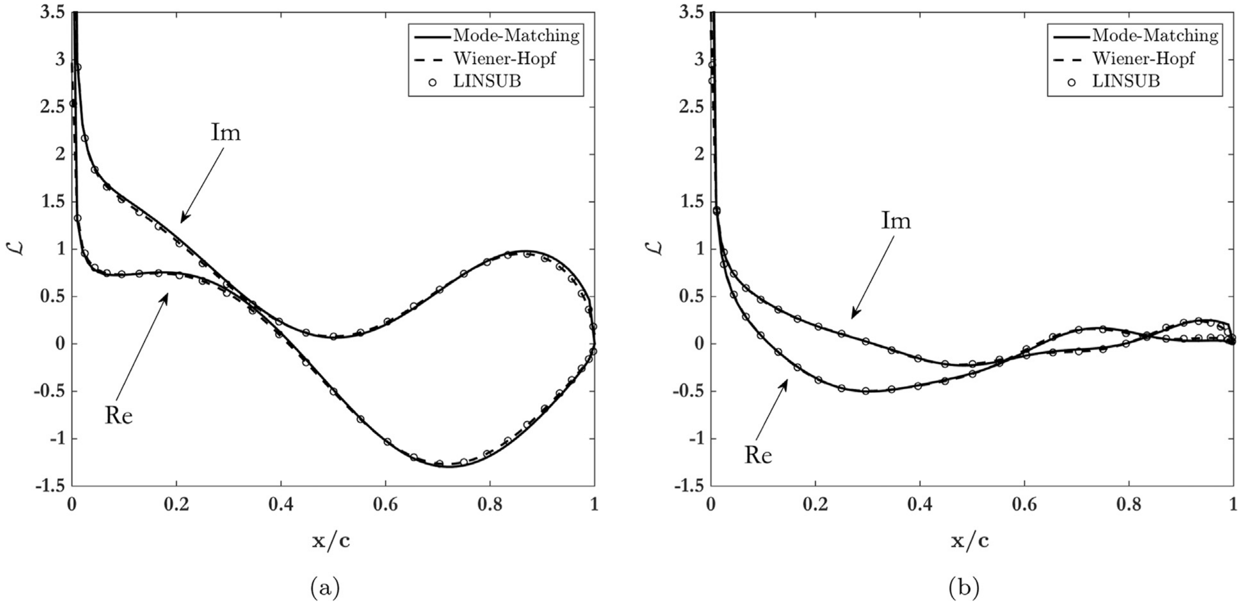

Fig. 13. Real and imaginary parts of the dimensionless pressure jumps for the test cases $u = \overline{k_x} = 5\pi/2$ (a) and $u = \overline{k_x} = 13\pi/2$ (b) from the mode-matching technique (plain), the Wiener-Hopf (dashed) technique and the LINSUB code (symbols).

Two configurations are considered: a low-frequency case with $u = \overline{k_x} = 5\pi/2$ and a high-frequency case with $u = \overline{k_x} = 13\pi/2$. Due to the azimuthal 2π-periodicity, these two cases correspond to the impingement of vortical gusts of 5 and 13 lobes, respectively.

4.3.2. Results

Figs. 11 and 12 report the instantaneous pressure and the modal amplitudes of the upstream-scattered ($|\mathbf{R}|$) and downstream-scattered ($|\mathbf{T}|$) waves. At the lower frequency ($\overline{k_x} = 5\pi/2$), only the mode $n + sV = 1$ is cut-on. The mean flow streches and contracts the wavefronts of the downstream and upstream waves, respectively. At the higher frequency ($\overline{k_x} = 13\pi/2$), four modes are cut-on. The mode $n + sV = -7$ dominates the upstream acoustic pressure field, whereas the energy is more distributed over the four modes downstream, as emphasized by inspection of Fig. 12-b and -c. The dominant modes are more easily identified by the numbers of wavefronts in the left-hand side parts of the field maps in Figs. 11-a and 12-a.

The field maps for both test cases are identical to those reported by previous investigators, for instance Durand and Hixon [58]. The real and imaginary parts of the dimensionless pressure jump across the reference vane (at $z = 0$) $\mathcal{L} = -\Delta p/(\rho_0 w_0 W_x)$ are plotted in Fig. 13. The results provided by the mode-matching technique are compared with those derived from the Wiener-Hopf technique [47] and from Smith's model [10], implemented by Whitehead [11] in the LINSUB code and applied to this specific test case by Hall [56]. A very good agreement between the three models is found for both the lower frequency (Fig. 13-a: $u = \overline{k_x} = 5\pi/2$) and the higher frequency (Fig. 13-b: $u = \overline{k_x} = 13\pi/2$).

A map of the instantaneous vorticity $\nabla \wedge \mathbf{v}^h$ for the test-case $u = \overline{k_x} = 5\pi/2$ is plotted in Fig. 14-a to assess the overall continuity of the prescribed gust. It is checked that the oblique wavefronts are uniformly reproduced in spite of the different expressions used in the various sub-domains. A profile of vorticity in the streamwise direction at $z/a = 0.5$ is shown in Fig. 14-b, where the expected sine pattern is perfectly synthesized. Finally profiles of vorticity according to the expressions of the gust in the unbounded domain ($\mathbf{v}_i^h$) and in the inter-vane channels ($\mathbf{v}_d^h$) along the leading-edge interface ($x = 0$) are compared in Fig. 14-c. The modal expansion of $\mathbf{v}_d^h$, from Eq. (32), exhibits sharp peaks in the immediate vicinity of the plates that have no consequence immediately away from the edges.

4.4. Application to rotor-stator interaction noise

The use of the proposed method to predict some key aspects of rotor-stator wake-interaction tonal noise is illustrated in this section on a configuration representative of a real low-speed axial-flow fan in an annular duct. The fan is made of a rotor with $B = 17$ blades and a stator of $V = 23$ outlet guide vanes. The calculations are carried out for an arbitrary cylindrical cut of radius R_0 between the hub and tip radii noted R_h and R_t, respectively. The solidity is $c/a = 1.25$, the axial Mach number is

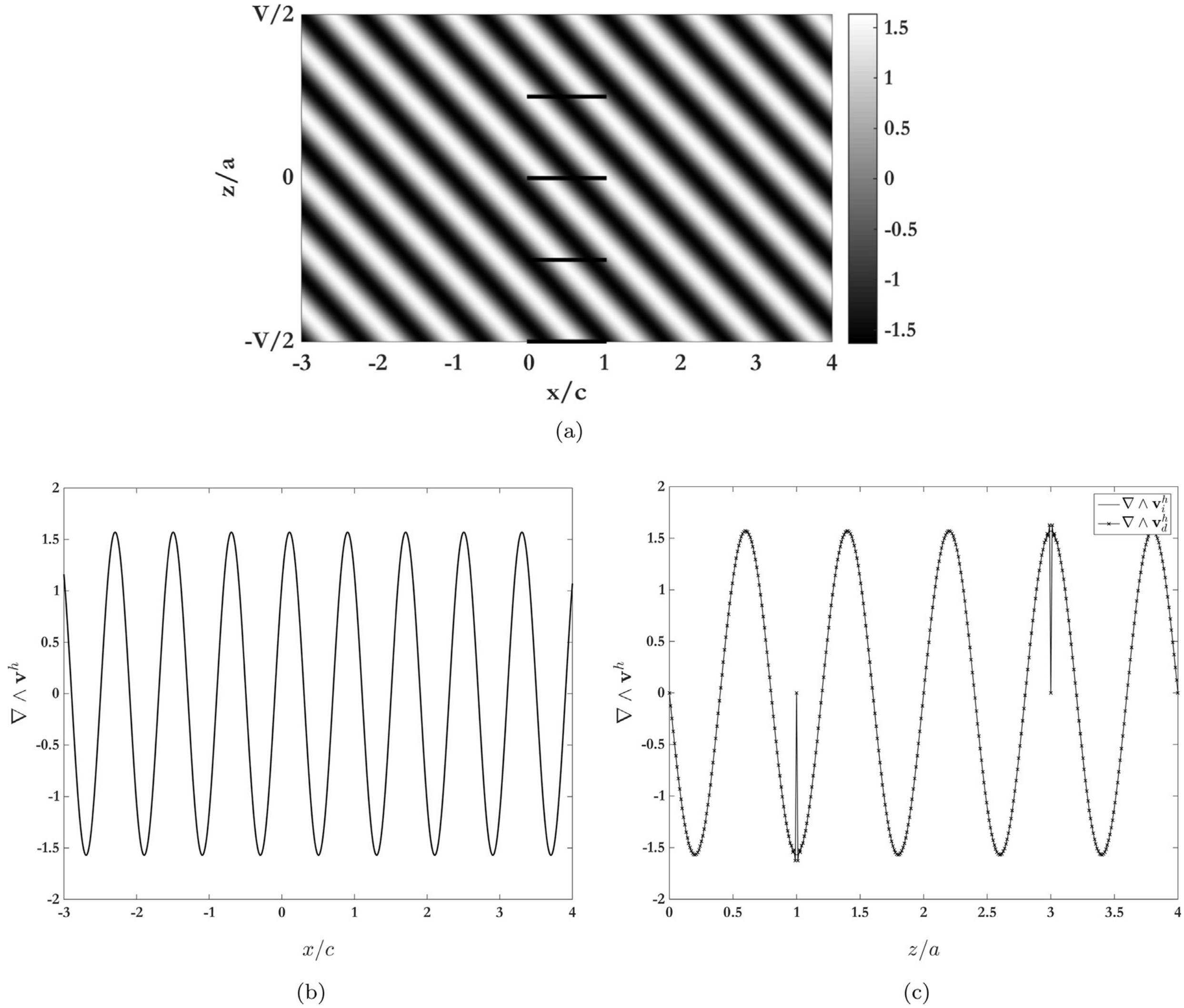

Fig. 14. Instantaneous vorticity of the gust prescribed in the mode-matching technique for $u = \overline{k_x} = 5\pi/2$. Vorticity map (a), and vorticity profiles in the streamwise direction at $z/a = 0.5$ (b) and along the leading-edge interface ($x = 0$).

$M = 0.06$ and the tangential Mach number of the blades is $M_t = \Omega R_0/c_0 = 0.3$. In fact the design is such that the first two tones at the BPF and its first harmonic (2BPF) are cut-off. Therefore the BPF ($n = 1$) and the first cut-on tone at 3BPF ($n = 3$) are selected here for the application. They correspond to the first and third Fourier components of the incident wake pattern. The test is mainly aimed at assessing how the cut-off and cut-on properties are reproduced. The results are reported in Figs. 15 and 16.

The instantaneous pressure field at the BPF is shown in Fig. 15-a in an arbitrary scale. The associated incident gust, traveling upwards in accordance with the conventions in Fig. 9, cannot be seen because it has no trace in terms of pressure. At the BPF, the rotor-stator interaction generates the dominant mode $n_i = nB \pm sV = 17 - 23 = -6$ expected from Tyler & Sofrin's rule and confirmed by the coefficient-bar charts in Fig. 15-b. This mode is counter-rotating, which means that the tangential phase speed of Mach number $-17M_t/6$ is downwards on the plot. In this case the total phase speed of the mode is subsonic, which can be expressed by $|nBM_t/(nB \pm sV)| < \beta$ and there is neither upstream nor downstream propagation. The amplitude of the mode is exponentially decaying from the interfaces, with nearly axially aligned pseudo-wave fronts. This corresponds to a cut-off mode (grey bar in Fig. 15-b). The cut-off modes do not carry acoustic energy but play an important role in the local continuity of the acoustic field. Along an axial distance δx, the decay of a cut-off mode reads

$$\exp\left\{-\frac{1}{\beta^2}\sqrt{\beta^2\alpha_s^2 - k_n^2}\,\delta x\right\}.$$

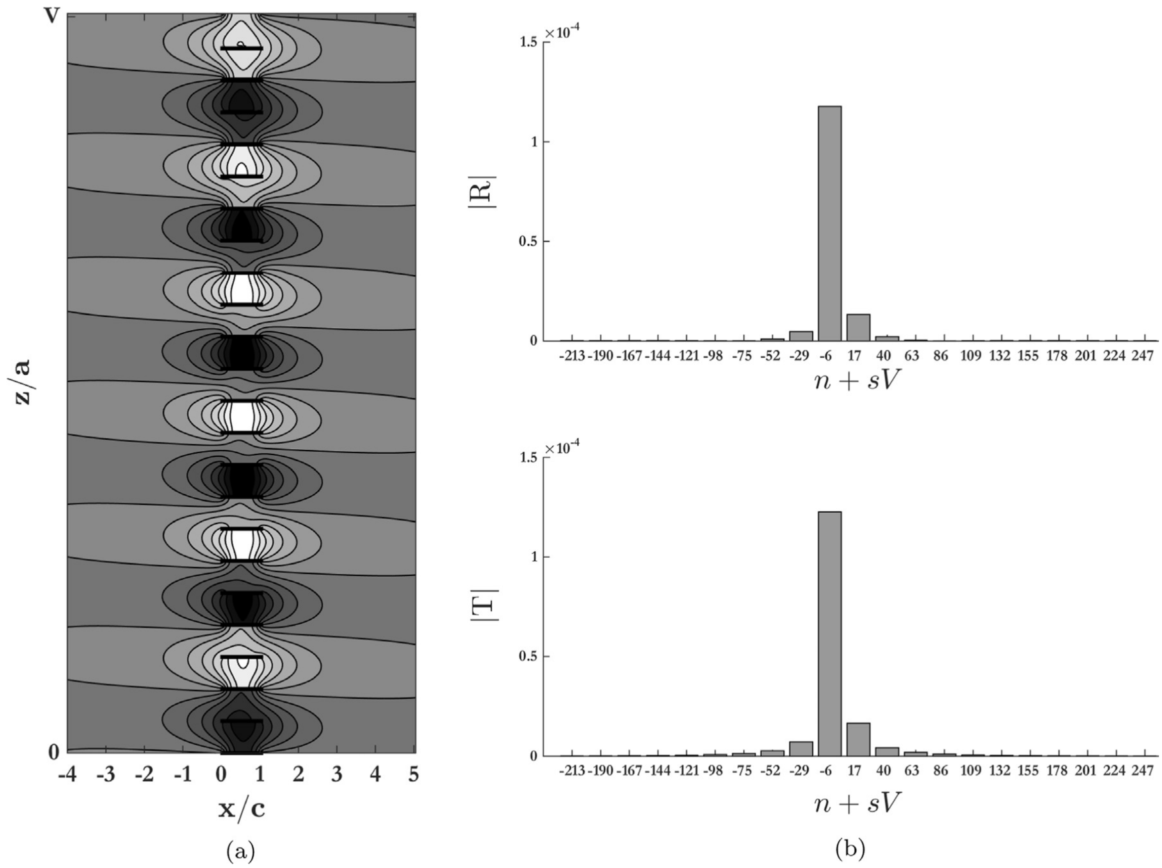

Fig. 15. (a): Instantaneous pressure field generated by gust impingement on the leading edge of an unwrapped cascade of vanes at the BPF ($n = 1$). Evidence of the cut-off mode $n_i = -6$. (b): Modal reflection $|\mathbf{R}|$ and transmission $|\mathbf{T}|$ factors. Gray bars denote cut-off modes.

It is faster as the azimuthal/tangential order increases, which explains that only the dominant mode $n_i = -6$ is visible in Fig. 15-a. The acoustic wavelength to chord-length ratio is $\lambda_n/c = 3.64$ ($\lambda_n = 2\pi/k_n$), the wavelength to channel-height ratio $\lambda_n/a = 4.54$ and the Helmholtz number $k_n R_0 = 5.07$. The inter-vane channels are acoustically compact in this case. Furthermore only the plane-wave mode is cut-on inside the inter-vane channels. Back and forth wave motion takes place in the channels between both interfaces, without energy loss but the one associated with the Kutta condition. With regard to the original annular geometry, this can be considered as a spinning trapped mode in the cascade.

At the third BPF ($n = 3$), as confirmed in Fig. 16, the rotor-stator interaction emits both upstream and downstream propagating oblique waves. These waves correspond to the dominant co-rotating mode $n_i = nB \pm sV = 3 \times 17 - 2 \times 23 = +5$ of supersonic tangential Mach number $51M_t/5$ in the unwrapped representation. The acoustic wavelength to chord-length ratio is $\lambda_n/c = 1.21$, the wavelength to channel-height ratio $\lambda_n/a = 1.51$ and the Helmholtz number $k_n R_0 = 15.20$. At this frequency, the vanes are not acoustically compact anymore and the scattering mechanism is much more complex. In terms of amplitude the only cut-on mode plotted as a black bar in Fig. 16-b is not dominant but it is the only one able to radiate away from the cascade. The other modes decay and only contribute in the vicinity of the cascade, both upstream and downstream.

In the present fan architecture, a special care was taken in the choice of the blade and vane counts to avoid the generation of the axial plane wave (mode of order 0) at the first two blade-passing frequencies. Whenever this mode exists, it is always cut-on whatever the frequency could be. With the present cascade model assuming zero-stagger plates, the axial plane-wave mode could never be excited because its equivalent acoustic sources would be dipoles tangentially oriented and in phase on all vanes. This is an inherent limitation of the current simplified geometry. The extension of the mode-matching technique to staggered cascades of plates is achievable, as suggested by Whitehead's work on electromagnetic waves [23]. It will be a crucial step in the future development of the methodology.

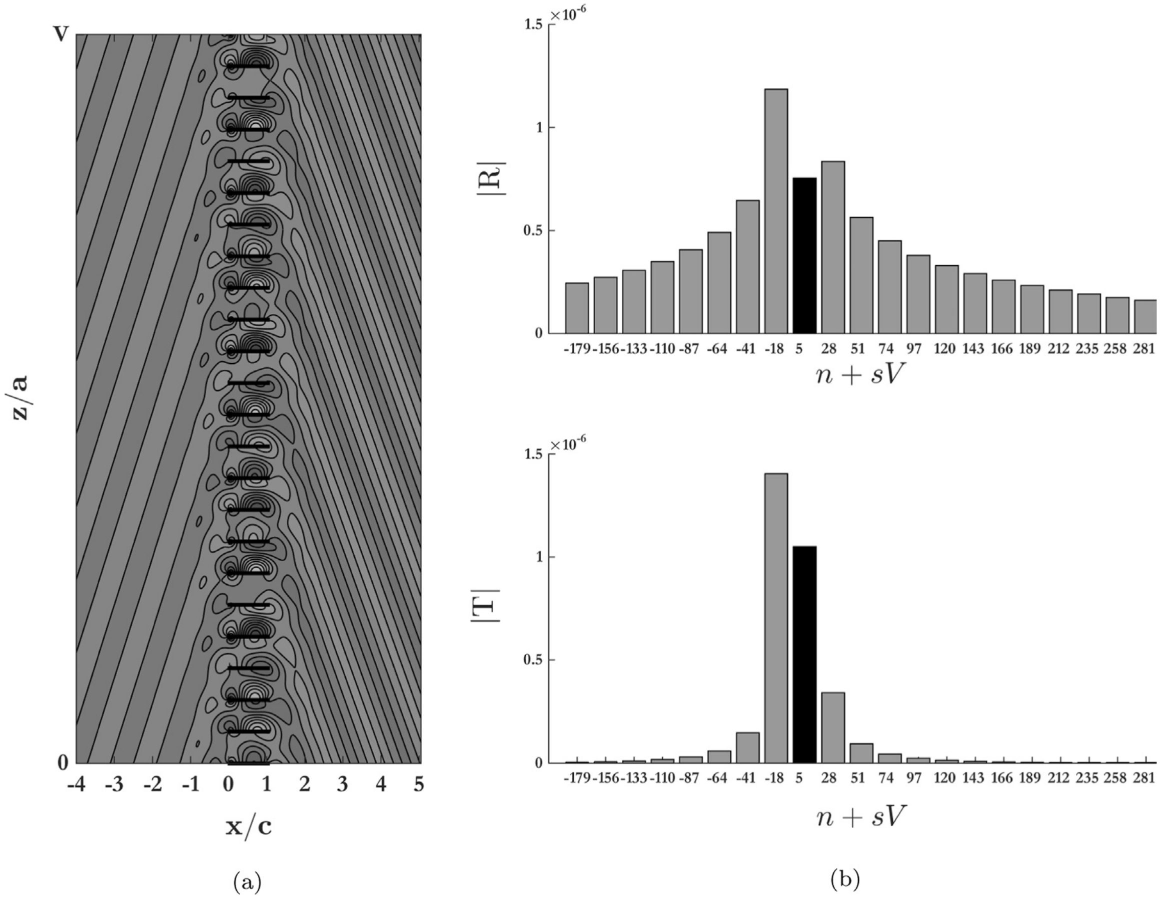

Fig. 16. (a): Instantaneous pressure field generated by gust impingement on the leading edge of an unwrapped cascade of vanes at the BPF harmonic $n = 3$. Evidence of the emission of the cut-on mode $n_i = +5$. (b): Modal reflection $|\mathbf{R}|$ and transmission $|\mathbf{T}|$ factors. Black and gray bars denote cut-on and cut-off modes respectively.

5. Conclusion

The present work establishes that the mode-matching technique is an efficient analytical prediction tool, not only for the sound transmission through a cascade of vanes but also for the sound generation by impingement of vortical disturbances on the vanes. The method consists in matching modal expansions of the acoustic and vortical fields at the leading-edge and trailing-edge interfaces, where the continuity of the fluctuating pressure and axial velocity is imposed. The multiple scattering by the leading-edge and the trailing-edge interfaces is reproduced by an alternate iterative solving of the matching equations at both interfaces, which reproduces the back-and-forth acoustic waves development in the bifurcated waveguides. The Kutta condition has been implemented, forcing a zero pressure jump at the trailing-edges of the vanes. Because of its effect, part of the acoustic energy of the incident wave is converted into hydrodynamic energy in the vane wakes. For this reason no energy balance can be written for the acoustic motion in the sound-transmission problem. In the sound generation problem the incident wave is specified as a pressure-free incompressible gust. The vorticity is carried along with the mean flow and assumed essentially frozen. It has a different expression as a sum of modes in the inter-vane channels, which introduces an additional set of unknowns in the problem. Apart from the continuity of pressure and axial velocity, the continuity of vorticity on both sides of an interface is also imposed to close the system of equations. The relevance of this approach is validated by comparisons with otherwise reported results on a benchmark of the NASA Second computational aeroacoustic workshop.

The two-dimensional mode-matching technique as described in the present paper for a cascade of zero-stagger vanes is mathematically equivalent to the Wiener-Hopf technique as applied by Glegg [16] and Posson et al. [20] as shown by comparisons between both methods. Its advantage is that it can be stated in a three-dimensional configuration of annular cascade of straight vanes, avoiding any strip-theory approach, which makes it a promising approach for turbomachinery aeroacoustics. Extensions are presently in progress. More generally the mode-matching technique can be used in any bifurcated waveguide system, provided that explicit modes for the convected Helmholtz equation are available is all subdomains of the system.

Acknowledgements

The present work is partially supported by the EC Project IDEALVENT (on the aeroacoustics of a generic air-conditioning system for aircraft) and by the FRAE in the French program SEMAFOR (on the enhancement of inverse microphone-array techniques in turbomachines by analytical source models). This work was also supported by the Labex CeLyA of Université de Lyon, operated by the French National Research Agency (ANR-10-LABX-0060/ANR-11-IDEX-0007).

References

[1] M.E. Goldstein, Aeroacoustics, McGraw-Hill, New York, 1976.
[2] H. Atassi, G. Hamad, Sound generated in a cascade by three-dimensional disturbances convected in a subsonic flow, in: Proceedings of the 7th AIAA Aeroacoustics Conference, 1981.
[3] K. Hall, P. Silkowski, The influence of neighboring blade rows on the unsteady aerodynamic response of cascades, in: Proceedings of the ASME 1995 International Gas Turbine and Aeroengine Congress and Exposition, American Society of Mechanical Engineers, 1995.
[4] N. Peake, A.B. Parry, Modern challenges facing turbomachinery aeroacoustics, Annu. Rev. Fluid Mech. 44 (2012) 227–248.
[5] T. von Kármán, W. Sears, Airfoil theory for non-uniform motion, J. Aeronaut. Sci., 5(10).
[6] S. Kaji, T. Okazaki, Propagation of sound waves through a blade row: II. Analysis based on the acceleration potential method, J. Sound Vib. 11 (3) . (355-IN1).
[7] S. Kaji, T. Okazaki, Generation of sound by rotor-stator interaction, J. Sound Vib. 13 (3) (1970) 281–307.
[8] F. Carta, Unsteady aerodynamic theory of a staggered cascade of oscillating airfoils in compressible flow, Report R-0582-19, U.A.C. Research Dept., 1957.
[9] D. Whitehead, Vibration and sound generation in a cascade of flat plates in subsonic flow. CUED/A-Turbo, Report CUED/A-Turbo/TR 15, Cambridge University Engineering Department, Cambridge, UK, 1970.
[10] S. Smith, Discrete frequency sound generation in axial flow turbomachines, Aeronautical Research Council Reports and Memoranda, R. & M. No. 3709.
[11] D. Whitehead, Classical two-dimensional methods, in: M. Platzer, F. Carta (Eds.), AGARD Manual on Aeroelasticity in Axial-Flow Turbomachines, Vol. 1, Unsteady Turbomachinery Aerodynamics, 1987, (Ch. 3).
[12] R. Mani, G. Horvay, Sound transmission through blade, J. Sound Vib. 12 (1) (1970) 59–83.
[13] W. Koch, On the transmission of sound waves through a blade row, J. Sound Vib. 18 (1) (1971) 111–128.
[14] N. Peake, The scattering of vorticity waves by an infinite cascade of flat plates in subsonic flow, Wave Motion 18 (3) (1993) 255–271.
[15] N. Peake, E. Kerschen, A uniform asymptotic approximation for high-frequency unsteady cascade flow, in: Proceedings of the Royal Society of London A: Mathematical, Physical and Engineering Sciences, vol. 449, The Royal Society, 1995, pp. 177–186.
[16] S. Glegg, The response of a swept blade row to a three-dimensional gust, J. Sound Vib. 227 (1) (1999) 29–64.
[17] H. Posson, M. Roger, S. Moreau, On a uniformly valid analytical rectilinear cascade response function, J. Fluid Mech. 663 (2010) 22–52.
[18] M. Namba, Three-dimensional analysis of blade force and sound generation for an annular cascade in distorted flows, J. Sound Vib. 50 (4) (1977) 479–508.
[19] H.M. Elhadidi, B. & Atassi, High frequency sound radiation from an annular cascade in swirling flows, in: Proceedings of the 8th AIAA/CEAS Aeroacoustics Conference and Exhibit, Breckenridge, Colorado, 2002, pp. 1–11.
[20] H. Posson, S. Moreau, M. Roger, On the use of a uniformly valid analytical cascade response function for fan broadband noise predictions, J. Sound Vib. 329 (18) (2010) 3721–3743.
[21] H. Posson, M.S., M. Roger, Broadband noise prediction of fan outlet guide vane using a cascade response function, J. Sound Vibr., 330, 2011, 6153–6183.
[22] R. Mittra, S.-W. Lee, Analytical Techniques in the Theory of Guided Waves, NY : Macmillan, New York, 1971.
[23] E. Whitehead, The theory of parallel-plate media for microwave lenses, Proc. IEE-Part III: Radio Commun. Eng., 98(52), 1951, 133–140.
[24] C. Linton, D. Evans, Acoustic scattering by an array of parallel plates, Wave Motion 18 (1) (1993) 51–65.
[25] D. Evans, Trapped acoustic modes, IMA J. Appl. Math. 49 (1) (1992) 45–60.
[26] Y. Duan, Trapped Modes and Acoustic Resonances (Ph.D. thesis), Loughborough University, 2004.
[27] Y. Duan, M. McIver, Rotational acoustic resonances in cylindrical waveguides, Wave Motion 39 (3) (2004) 261–274.
[28] A. Nayfeh, D. Huddleston, Resonant acoustic frequencies of parallel plates, AIAA Paper, 1979, 79–1522.
[29] R. Parker, Resonance effects in wake shedding from parallel plates: calculation of resonant frequencies, J. Sound Vib. 5 (2) (1967) 330–343.
[30] W. Koch, Resonant acoustic frequencies of flat plate cascades, J. Sound Vib. 88 (2) (1983) 233–242.
[31] M. Roger, Analytical modelling of wake-interaction noise in centrifugal compressors with vaned diffuser, in: Proceedings of the 10th AIAA/CEAS Aeroacoustics Conference, Manchester, 2004, p. 2994.
[32] M. Roger, S. Moreau, A. Marsan, Generation and transmission of spiral acoustic waves in multi-stage subsonic radial compressors, in: Proceedings of the 20th AIAA/CEAS Aeroacoustics Conference, 2014.
[33] J. Ingenito, M. Roger, Analytical modelling of sound transmission through the passage of centrifugal compressor, in: Proceedings of the 13th AIAA/CEAS Aeroacoustics Conference, 2007.
[34] I. Evers, N. Peake, On sound generation by the interaction between turbulence and a cascade of airfoils with non-uniform mean flow, J. Fluid Mech. 463 (2002) 25–52.
[35] S. Bouley, B. François, M. Roger, H. Posson, S. Moreau, On a mode-matching technique for sound generation and transmission in a linear cascade of outlet guide vanes, in: Proceedings of the 21st AIAA/CEAS Aeroacoustics Conference, vol. 2825, 2015.
[36] M. Roger, B. François, S. Moreau, Cascade trailing-edge noise modeling using a mode-matching technique and the edge-dipole theory, J. Sound Vibr.
[37] H. Posson, H. Beriot, S. Moreau, On the use of an analytical cascade response function to predict sound transmission through an annular cascade, J. Sound Vib. 332 (15) (2013) 3706–3739.
[38] C. Chapman, Sound radiation from a cylindrical duct. Part 1 ray structure of the duct modes and of the external field, J. Fluid Mech. 281 (05) (1994) 293–311.
[39] A.J. Cooper, N. Peake, Upstream-radiated rotor-stator interaction noise in mean swirling flow, J. Fluid Mech. 523 (2005) 219–250.
[40] A. Pierce, Acoustics: An Introduction to its Physical Principles and Applications, McGraw-Hill Book Company, New York, 1981.
[41] A.P. Dowling, J.E.Ffowcs Williams, Sound and Sources of Sound, Horwood, UK, 1983.
[42] G. Floquet, Sur les équations différentielles linéaires à coefficients périodiques, Ann. Sci. de l'École Norm. Supérieure 12 (2) (1883) 47–88.
[43] D. Jones, Aerodynamic sound due to a source near a half-plane, IMA J. Appl. Math. 9 (1) (1972) 114–122.
[44] S. Rienstra, Sound diffraction at a trailing edge, J. Fluid Mech. 108 (1981) 443–460.
[45] M.S. Howe, Attenuation of sound due to vortex shedding from a splitter plate in a mean flow duct, J. Sound Vib. 105 (3) (1986) 385–396.
[46] S. Job, E. Lunéville, J.-F. Mercier, Diffraction of an acoustic wave by a plate in a uniform flow: a numerical approach, J. Comput. Acoust. 13 (4) (2005) 689–709.

[47] H. Posson, Fonctions de réponse de grille d'aubes et effet d'écran pour le bruit à large bande des soufflantes (Ph.D. thesis), École Centrale de Lyon, 2008.
[48] H. Posson, M. Roger, Parametric study of gust scattering and sound transmission through a blade row, in: Proceedings of the 13th AIAA/CEAS Aeroacoustics Conference, 2007.
[49] B.-T. Chu, L.S. Kovásznay, Non-linear interactions in a viscous heat-conducting compressible gas, J. Fluid Mech. 3 (5) (1958) 494–514.
[50] M. Roger, Sur l'utilisation d'un modèle de sillages pour le calcul du bruit d'interaction rotor-stator, Acta Acust. United Acust. 80 (3) (1994) 238–246.
[51] B. Reynolds, B. Lakshminarayana, A. Ravindranath, Characteristics of the near wake of a compressor of a fan rotor blade, AIAA J. 17 (9) (1979) 959–967.
[52] J.M. Tyler, T.G. Sofrin, Axial flow compressor noise studies, Tech. rep., SAE Technical Paper, 1962.
[53] D. Lockard, P. Morris, A parallel simulation of gust/cascade interaction noise, in: C. Tam, J. Hardin (Eds.), Proceedings of the Second Computational Aeroacoustics (CAA) Workshop on Benchmark Problems, Vol. NASA-CP-3352, 1997, pp. 279–287.
[54] C. Tam, K. Kurbatskii, J. Fang, Numerical boundary conditions for computational aeroacoustics benchmark problems, in: C. Tam, J. Hardin (Eds.), Proceedings of the Second Computational Aeroacoustics (CAA) Workshop on Benchmark Problems, Vol. NASA-CP-3352, 1997, pp. 191–219.
[55] F. Hu, J. Manthey, Application of PML absorbing boundary conditions to the benchmark problems of the computational aeroacoustics, in: C. Tam, J. Hardin (Eds.), Proceedings of the Second Computational Aeroacoustics (CAA) Workshop on Benchmark Problems, Vol. NASA-CP-3352, 1997, pp. 119–151.
[56] K. Hall, Exact solution to category 3 problems – turbomachinery noise, in: C. Tam, J. Hardin (Eds.), Proceedings of the Second Computational Aeroacoustics (CAA) Workshop on Benchmark Problems, Vol. NASA-CP-3352, 1997, pp. 41–43.
[57] K. Hall, A variational finite element method for computational aeroacoustic calculations of turbomachinery noise, in: C. Tam, J. Hardin (Eds.), Proceedings of the Second Computational Aeroacoustics (CAA) Workshop on Benchmark Problems, Vol. NASA-CP-3352, 1997, pp. 269–278.
[58] C. Durand, D. Hixon, Comparison of computational aeroacoustics prediction of vortical gust scattering by a 2d stator with flat plate theory, in: Proceedings of the 21st AIAA/CEAS Aeroacoustics Conference, 2015, p. 2842.